A Novel System for the Measurement of Dynamic Loading on a Bicycle Frame

by

Ryan A. Consell

A thesis
presented to the University of Waterloo
in fulfillment of the
thesis requirement for the degree of
Master of Applied Science
in
Mechanical Engineering

Waterloo, Ontario, Canada, 2013

AUTHOR'S DECLARATION

I hereby declare that I am the sole author of this thesis. This is a true copy of the thesis, including any required final revisions, as accepted by my examiners.

I understand that my thesis may be made electronically available to the public.

Abstract

The design of bicycle frames has remained fairly static for the majority of the past century, but recent increases in demand for high performance bicycles has created an accelerated design cycle that requires innovation. In order to design new frames with confidence in their capacity to withstand the rigors of use, reliable data about the nature of that use is needed, but this data is not currently available. The purpose of this research was to develop and implement a system that is capable of interpolating loads applied to a bicycle frame during vigorous riding for the purpose of improving the quality of information available to bicycle designers.

The system that was developed employed finite element modeling to locate strain gauges on a frame and a least-squares approximate solution of strain readings to interpolate the applied loads. At its best, the system is capable of resolving loads with better than a 2% error. This system is limited, though, as it can only be applied in cases where the frame has a significant strain reaction to a load case but does not have a significant change in geometry during loading. This system was implemented on a cross-country mountain bicycle frame for the purposes of determining a rider weight to load relationship and to compare the standardized test procedures for bicycles to the loads experienced in the field.

It was confirmed that there is a linear relationship between rider weight and load on the frame for all component forces except that applied to the bottom bracket, out of plane with the bicycle frame. It was also found that the British Standards fatigue testing practices, which are used internationally to assess bicycle safety, are inconsistent in their representation of realistic riding conditions when compared with the results from the field tests. Some loads appear conservative, some offer a very large factor of safety, and two are not represented at all. In particular, the moment about the bottom bracket due to pedaling and the load on the seat from the rider appear to consistently exceed the standardized test requirements while the moment caused by fork splay seems much smaller than the tests demand.

Acknowledgements

I would like to thank Professor Sanjeev Bedi and Professor Mahesh Pandey for their support and guidance throughout my research.

I would like to acknowledge Ali Saeed, my partner on the early portions of this research for his time, effort, and valuable insights. This project would not have succeeded without him.

I would also like to thank Joanne Hughes at Rocky Mountain Bicycles and Richard Matthews at Vroomen White Design for their support of the research.

Finally I would like to Thank Andy Cox and the team at King Street Cycles for lending their riding skill and maintenance expertise to the project.

Thank you all.

Table of Contents

List of Figures

List of Tables

Chapter 1
Introduction

1.1 Background

Cycling is one of the most popular recreational sports in the world and is growing as a means of commuting in city centers. The sale of bicycles, accessories and related gear is in excess of six billion dollars annually in North America alone [1]. The basic bicycle design has remained static for much of the previous century, however recent advancements in materials science and manufacturing processes, including the introduction of aluminum alloys and carbon fiber, as well as the inclusion of suspension, have accelerated the development cycle for new bicycles. Also, the popularity of a variety of competitive race styles including road, mountain, cross-country, downhill, and more have created a demand for innovative and highly specialized designs.

In order to meet these demands, new models are developed regularly. For reduced lead time between design and sales, finite element modeling (FEM) has been broadly adopted by bicycle frame designers. However, in order for these models to be of value, meaningful load cases are required.

Currently, the standard practice employs various loads required by the European Standards [2] [3] [4] which provide guidelines for impact and fatigue tests needed to validate the safety of a new design for release on the European market. These do not, however, consider aspects that affect the performance of a bicycle such as stiffness. It is also not clear to bicycle designers whether these tests accurately represent the loads applied to their bicycles by riders of different skill, size and weight. Consequently, there is a need for an accurate model of rider induced loads onto a bicycle frame so that those conditions can be incorporated into the design process.

1.2 Project motivations

The intention of this project is to develop a system through which all major loads being applied to a bicycle frame can be measured. This system is to be used on a variety of bicycle frames for the purpose of developing meaningful data on the loads being applied to bicycle frames under actual riding conditions.

The overall aim is to create a model of extreme and expected loads that a bicycle can expect to see based on the biometrics of the rider and the nature of the riding (road, mountain, stunt, etc.)

The expectation is that this data can be used to inform the design process of new bicycle frames for the purposed of performance, durability and comfort as well as give insight into warranty periods and pricing.

1.3 Problem Statement

To develop and implement a system by which all significant loads applied to a bicycle frame during riding can be measured at a rate high enough to capture all significant events over a period long enough to capture a full trail ride which includes accelerating, braking, maintaining speed and coasting.

The system will need to be light enough so as to not seriously impact the performance of the rider. It must also not require any meaningful change to the bicycle components in their function, strength or geometry and it must be possible to apply the system to a variety of bicycle frame geometries.

The system is to be used to collect data from a variety of riders. These data are to be used to determine fatigue loading through rainflow analysis, extreme load cases, and statistical models for riding events including pedaling and braking.

1.4 Thesis Layout

This thesis will begin with an exploration into similar work that has been published which will serve as a basis for further discussion as well as helping to identify the current gap in published documentation which this thesis aims to fill. Following the literature review, the fundamental theory upon which the measurement system is being based will be discussed.

With the background firmly established, the development process of the system will be detailed including proof of concept testing, initial applications, tests and revisions, final implementation, and suggestions for future improvement and a discussion of other applications in which a similar system could be effectively implemented. This section will also include an analysis and discussion of the accuracy of the system.

Next, the field tests will be detailed. This section will include summaries of the nature of the rides, riders and raw results of these tests.

The next sections will involve analysis of the test data. The focus will be on developing a model of applied loads based on rider weight and discussing the results of this model as compared to the standardized tests for bicycle safety.

The final section will include a discussion of other directions that could be taken following from the current research and a summary of the findings and conclusions of the project.

1.5 Definition of Terms

1.5.1 Bicycle Components

Figure 1: Bicycle Components [5]

1. Seat or saddle – Where the rider sits
2. Seat post – Connects the saddle to the frame, usually has adjustable height
3. Seat tube – Part of the frame into which the seat post is inserted
4. Top tube – Horizontal structural member of the frame
5. Stem – Part of the fork assembly that extends through the head tube
6. Head tube – Frame member that supports the front fork and handlebar assembly
7. Down tube – Lower structural member of the frame
8. Crank arm – Component that connects the pedal to the crank assembly
9. Seat stay – Structural member of the frame between rear dropout and seat tube

10. Chain – Transfers power from crank assembly to rear wheel
11. Fork – The assembly to which the front wheel is mounted
12. Chain stay – Structural member of the frame between rear dropout and bottom bracket
13. Bottom Bracket – Section of the frame through which the crank assembly is mounted
14. Chainrings – the sprockets connected to the crank assembly
15. Front shock – The shock absorbers, typically pneumatic, in the fork
16. Rear Dropout – The part of the frame to which the rear wheel is mounted
17. Derailleur – Mechanical system that shifts the chain between sprockets, front and rear
18. Brakes – Mechanical braking system, can be disk or hub brakes, includes front and rear.
19. Rear Shock – The shock absorber for the rear wheel
20. Handlebars – Cross bar which the rider uses to steer.

1.5.2 Applied Loads

There are a number of loads that can be applied to the bicycle frame. For convenience, a series of shorthand reference labels were developed by which to identify them. Figure 2: Relevant Load Labels shows the labels given to the various load points. Note that most of the loads follow a Cartesian coordinate system but the chain and the brake load are applied in their own, unique directions.

Also, while the chain force, bottom bracket (BB) forces and the head tube (HT) forces will remain in the same location for all bicycles; different configurations can have slightly different seat force locations and very different brake force locations.

Figure 2: Relevant Load Labels [6]

Chapter 2
Review of Literature

2.1 Instrumentation

The bicycle is by no means a new device and has been studied academically as far back as 1869 [7]. Studies of dynamics, kinematics, control and more have been carried out, but much of these studies were theoretical or worked on simplified models due to the difficulties taking in-situ measurements on a bicycle in use. Developments in computer and instrumentation technology in the 1990s allowed for new approaches to the science and a great deal of work has gone into the development of methods for gathering and analyzing data on bicycles.

Most component parts of a bicycle have had custom instrumentation designed. Hull [8] [9] [10] and Champoux [11] have put significant effort into the development of instruments to gather data from loads applied to pedals. They have independently created six axis pedal dynamometers capable of recording the force and position applied to each pedal. These showed excellent ability to collect precise force and motion data from riders, but required specialized pedals to be built.

Hull [12] and Champoux [13] also created systems for measuring wheel loads at the hubs of bicycle wheels. These are capable of resolving the three orthogonal forces applied to each dropout during riding. There is a limitation on these designs, though, in that they require the modification of the frame components.

Handlebars have also been instrumented for determination of fatigue loading characteristics by Hull [14]. This system employed strain gauges on the handlebars and was successfully used to investigate off-road cycling conditions and confirm fatigue loading models for the handlebars. This supports the effectiveness of using strain gauges to analyze bicycle loading.

Champoux also developed a complete system for collecting seat, pedal, handlebar and hub loads on an off-road bicycle [15]. While effective and had similar end-goals to the project in this paper, this system relied on attaching modified components to the bicycle and altering the frame. This approach also required a wide variety of instrumentation solutions which adds the challenge of monitoring and synching disparate data sources.

Giannetti implemented a system using strain gauges to monitor the stress distribution throughout a racing bicycle frame [16]. This system demonstrates several features ideal for analysis of high-performance bicycles. First, it is lightweight; strain gauges and their associated wiring have negligible mass. Second, it does not alter the components or the profile of the bicycle. Finally, it is

relatively inexpensive as strain gauges are a relatively low-cost sensor. These attributes make the system attractive; however it is only capable of interpreting stress distributions in the frame. This method, though, could be used as a basis for a system for measuring the forces being applied to the frame if a means of interpolating between the strain readings and the applied loads can be found.

2.2 Load Testing

Many attempts have been made to determine the loads experienced by bicycles during riding. These are frequently divided into surface induced loads and rider induced loads. The current project does not make a specific distinction between them as all loads impacting the bicycle frame are of interest, but it is useful to investigate the results of other studies.

Soden and Adeyefa were able to determine normal and shear loads on bicycle pedals, saddle and handlebars while accelerating both seated and standing. Through their tests, they determined that during normal riding, 50% of rider weight is supported by the saddle and the other 50% moved between pedal and handlebar throughout the pedal stroke. While accelerating or climbing, the rider applied more than twice their body weight to the forward pedal and accompanied a pull on the handlebars that exceeded body weight. The maximum load measured in these cases was at the pedal and reached nearly three times body weight of the rider. [17] This study gives good baseline values to expect from rider induced loads but was carried out on smooth surfaces and makes no comment on terrain effects.

Lorenzo and Hull were able to expand on these observations with measurements of reaction forces in the wheel hubs. Their results indicate similar results to those above but found that terrain effects can increase the load on the pedals and both wheels to five times rider weight. Through experimental tests, they accumulated information on the mean loads and distribution of loads expected from the handlebars, front and rear hubs, and vertical and tangential forces on the pedals. They also presented a correlation coefficient between each force to assist with fatigue analysis. [18] These are useful results for reference. However, they omit the effect of the rear brake and saddle.

Stone and Hull investigated the relationship between rider weight and induced loads on bicycles. They determined that in all tested ride circumstances, which included a variety of inclines and pedaling rates with riders of different weight and skill level, the normal pedal load followed a linear relationship with rider weight. [19] This was considered an important finding as the normal force applied at the pedal is the dominant contributor to fatigue failure [20]. It is also a useful reference for evaluating the system being developed.

Hölzel, Hoechtl and Senner did preliminary investigations into the impact of possible predictable misuse scenarios on bicycles including impacting obstacles poorly, landing from large drops, and riding on destructively rough terrain. Their results imply that these loads can easily exceed double the normal peaks from normal use. [21] This is an important consideration when designing a load measurement system expecting to be used in the field. The range of measurements and durability of the system must be able to meet these potential extreme demands.

All of the research done to date provides good information on individual component forces, but leaves an important gap in knowledge. A method of measuring all forces applied to a frame synchronously has not yet been demonstrated. With such a method, complete load cases could be discerned which can be meaningfully applied to design practices to ensure the strength and stiffness desired in a bicycle frame. In addition, such a system could give insight into the variable loads experienced by the frame and applied to create fatigue testing protocols that better represent real-world riding.

Chapter 3
Theory

There are three basic assumptions being employed in the system being developed. Each will be introduced and discussed in this section and experimentally verified in later sections.

The first assumption is that an applied mechanical load ($P_{applied}$) to a bicycle frame can be calculated by measuring the strain (ε) at a discrete location on that frame.

$$\varepsilon = f(P_{applied}) \quad \text{(eq. 1)}$$

The second assumption is that under normal operating conditions, the strain experienced by the components of the frame are well below the yield limit of the material and have a linear relationship between applied load and strain.

$$\varepsilon = kP_{applied} \quad \text{(eq. 2)}$$

The final assumption is that the strain at any discrete location caused by multiple loads simultaneously will be the linear sum of the independent force-strain relationships.

$$\varepsilon = k_1P_1 + k_2P_2 + k_3P_3 \ldots \quad \text{(eq. 3)}$$

If all of these assumptions are correct then it will be possible to determine what loads are acting on a bicycle frame by interpreting the resulting strain at several discrete locations. To accomplish this, at least as many strain gauges as there are component input forces need to be applied to the frame. Next, the load-to-strain, or stiffness, coefficient (k) for each strain gauge under each component load must be experimentally determined.

With each stiffness coefficient (k_{mn}) evaluated, a set of linearly independent equations can be formed relating the component forces (P_n) to the strains at each gauge (ε_m).

$$\begin{aligned} \varepsilon_A &= k_{1A}P_1 + k_{2A}P_2 + k_{3A}P_3 + \cdots + k_{nA}P_n \\ \varepsilon_B &= k_{1B}P_1 + k_{2B}P_2 + k_{3B}P_3 + \cdots + k_{nB}P_n \\ &\vdots \\ \varepsilon_m &= k_{1m}P_1 + k_{2m}P_2 + k_{3m}P_3 + \cdots + k_{nm}P_n \end{aligned} \quad \text{(eq.4)}$$

Or, written in matrix form

$$\varepsilon = k \quad P \quad \text{(eq. 5)}$$

If there are an equal number of strain gauges and component forces, then [k] will be a square matrix and therefore easily invertible. Thus, given a set of strain readings it is possible to determine the loads being applied.

$$P = k^{-1} \varepsilon \quad \text{(eq. 6)}$$

However, a system of this kind can be difficult to apply as there is no obvious way to construct a layout of strain gauges that would ensure a linearly independent [k], and system noise from vibrations traveling through the bicycle could introduce large errors. A possible way to mitigate this is to apply more strain gauges than needed. This would generate an over-determined system of equations that could be used to create a least-squares, best-fit solution.

Starting with eq.5 where [ε] and [P] are vector matrices and [k] is a rectangular matrix of stiffness coefficients containing more columns than rows, if both sides of equation are multiplied by a transpose of [k],

$$k^T \epsilon = k^T k P \quad \text{(eq. 7)}$$

An invertible square matrix can be formed by the multiplication of $[k]^T[k]$. By multiplying both sides of eq. 7 by the inverse of $[k]^T[k]$, we can solve for [P]

$$P = k^T k^{-1} k^T \epsilon \quad \text{(eq. 8)}$$

This equation is a well-known least squares approximation used for over-determined systems [22]. The matrix formed by $([k]^T[k])^{-1}[k]^T$ will be referred to as [j] for simplicity.

This [j] matrix provides the tool for translating between strain measurements in discrete locations and compound loads applied to an object displaying linear-elastic behavior. The next stage in development is to attempt to apply this theory in a simple physical model to verify the effectiveness and accuracy. If the system is shown to be valid in a simple application, it can then be expanded to a full bicycle frame.

3.1 Proof of Concept

The initial investigation into the efficacy of the [j] matrix methodology was carried out on the simplest system that could be constructed with the resources at hand. A thin-walled aluminum pipe was considered to be a reasonable analogue for an aluminum bicycle frame. Six linear strain gauges were attached to a pipe as shown in Figure 3.

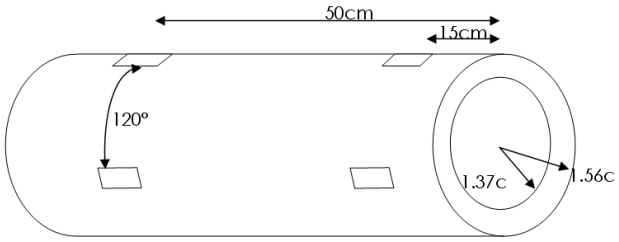

Figure 3: Aluminum Cantilever Beam Schematic

The pipe was then mounted to a rigid steel frame with one end constrained in all directions and the other left free thus creating a cantilever beam system. The steel frame was also fitted with pulleys and steel ropes to allow the free end of the pipe to be pulled in the three primary Cartesian directions (Figure 4, Figure 5). Not shown in the figures is the cable running through the pipe which loads the pipe in compression.

For convenience, the strain gauges were given labels by their location. Those close to the fixture were labeled “proximal” those near the free end of the pipe were called “distal”. The ones facing upwards were labeled “top”. Those located 120° clockwise from the top when observed from the free end were labeled “right” and those 120° counterclockwise were labeled “left”.

Figure 4: Aluminum Cantilever Beam

Figure 5: Aluminum Cantilever Beam with Vertical and Side Loads Applied

3.1.1 Testing Linearity

In order to test the efficacy of the [j] matrix system, it is first necessary to establish that the object being tested has a linear load-strain response. To verify this, the pipe was loaded in each of the three Cartesian directions separately over unit load increments of 5N. The results of the vertical load test are shown in Figure 6.

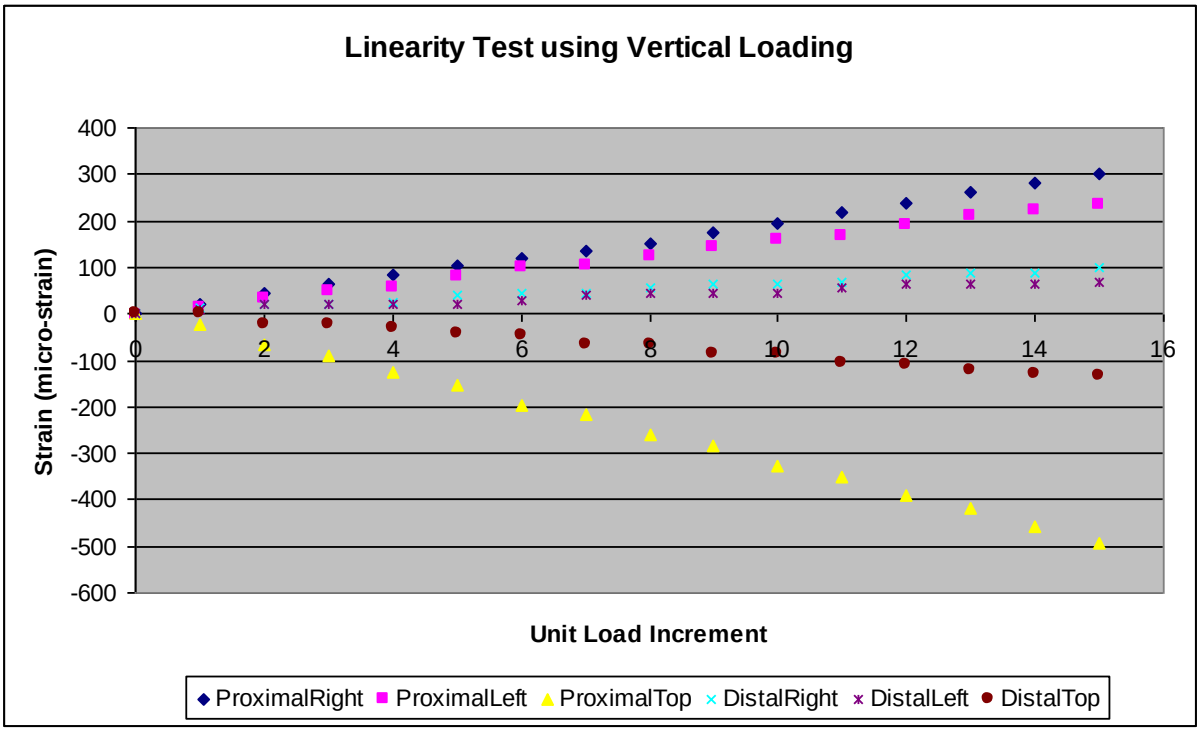

Figure 6: Linearity Test of Aluminum Cantilever Beam in the Vertical Direction

A summary of all of the tests are shown in Table 1 in terms of the R^2 linear regression. When loaded in bending, the response is highly linear. However, under compression and when the strain gauge is located along the neutral axis of the bend, the reaction in the strain gauges was very small in an absolute sense and also low with respect to the signal-to-noise ratio of the system and therefore resulted in poor linearity.

Table 1: Summary of R^2 Linearity Tests on Cantilever Beam

	x1	x2	y1	y2	z1	z2
ProximalRight	0.993	1.00	0.999	1.00	**0.409**	**0.434**
ProximalLeft	0.996	0.991	0.998	0.996	**0.225**	**0.252**
ProximalTop	**0.302**	**0.863**	0.999	1.00	**0.444**	**0.454**
DistalRight	0.983	0.963	0.979	0.976	**0.326**	**0.447**
DistalLeft	0.985	0.975	0.965	0.97	**0.345**	**0.309**
DistalTop	**0.167**	**0.671**	0.992	0.987	**0.271**	**0.398**

This is an important result as it indicates that strain gauges must be located in such a way as to have a strong response from a load case, or k value, in order to be valuable for the [j] matrix

method. A corollary of this is that any load case that does not have a location on the base frame with a large k value cannot be effectively interpreted by this method.

3.1.2 Verifying the [j] Matrix

Using the slopes of each of the reactions to the applied loads, [k] was measured and then [j] calculated for the cantilever beam system. Known loads were then applied to the beam and compared to the values calculated by measuring the strains and using eq. 8. Twelve such tests were carried out, four in each loading direction. Table 2 shows the results of one of these tests, which was typical.

Table 2: Sample Load Comparison Test for Cantilever Beam

	Actual	Calculated
Fx	6	5.93
Fy	0	0.04
Fz	0	-1.4

These were typical error magnitudes for all test cases. It was found that the x and y components of load could be resolved to within 2% of the total applied load on the beam while the z component, that is the component in compression along the length of the pipe, had upwards of 30% error with respect to the magnitude of the applied load.

A similar test was carried out wherein a load was applied in an arbitrary direction and the resultant strains measured. Then, using the loads resolved from eq. 8, the fixture was loaded in each of the component directions in an attempt to replicate the strain reaction caused by the arbitrary load. The goal in this was to determine if the process would be able to break down an unknown load case into its components effectively such that it could be replicated on a fixture. This test yielded similar results to the earlier, individual component load tests.

3.2 Implementation on Vertex

With the efficacy of the basics of the system verified using the cantilever beam, it was time to attempt to apply the system to a bicycle frame. Rocky Mountain Bicycles (RMB) provided a hardtail (no rear suspension) Vertex model aluminum frame (Figure 7). It was an older model cross-country frame that had the paint stripped off for previous experiments.

Figure 7: Vertex Hardtail Frame [23]

3.2.1 Locating Strain Gauges

The first step in applying the [j] matrix system to a bicycle frame was determining a method by which to locate the strain gauges. On the cantilever beam, the single loading point and simple geometry meant that hand calculations could predict where the strain reactions would be highest. The bicycle frame, however, has a complex geometry including hydroformed tubes, asymmetry and welded joints. Also, there would be several loading points. This complexity made it impractical to attempt to determine key areas of strain analytically so finite element modeling (FEM) was employed.

Rocky Mountain Bicycles had finite element models for their frames and cooperated in running analyses on them for the purposes of this project. Four case-loads (Figure 8- Figure 10) were applied using the analysis and constraints typically used by RMB and are based on the mountain bicycle safety requirements that manufacturers selling in Europe need to abide [2].

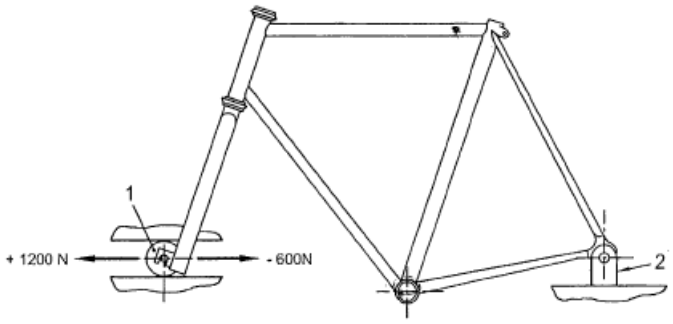

Key

1 Free-running guided roller

2 Rigid, pivoted mounting for rear axle attachment point

Figure 8: 1200N Fork Splay Load Case [2]

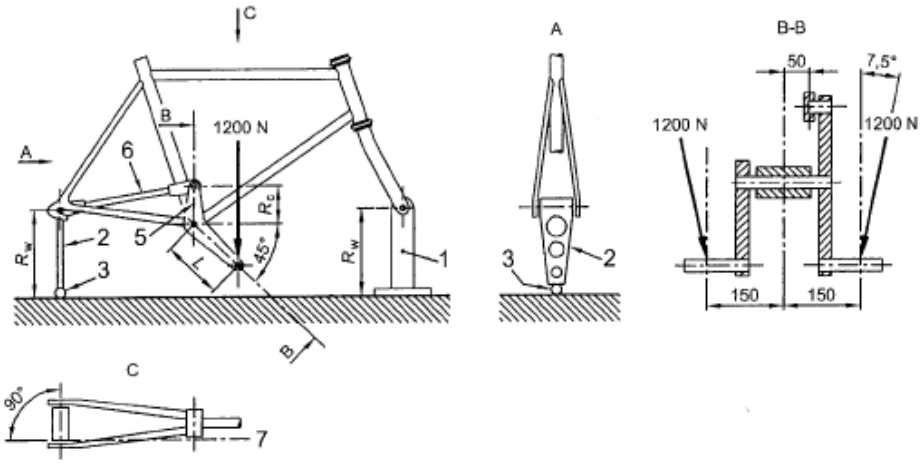

Key

R_w Height of rigid mount and vertical link

R_c Length of vertical arm (75 mm)

L Length of crank replacement (175 mm)

1 Rigid mount

2 Vertical link

3 Ball-joint

4 Adaptor assembly

5 Vertical arm

6 Tie-rod

7 Centre-line of tie-rod

Figure 9: 1200N Pedal Load Cases [2]

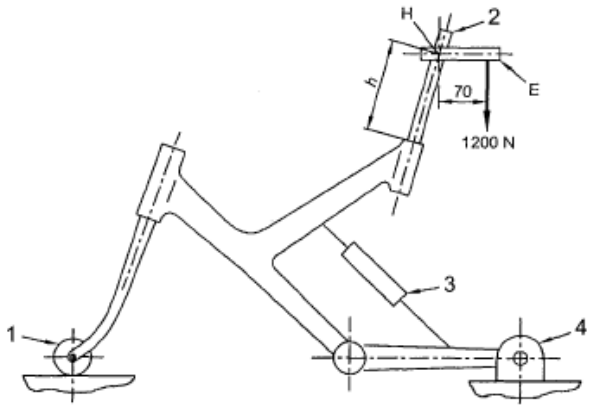

Key

1 Free-running roller
2 Steel bar
3 Locked suspension unit or solid link for pivoted chain-stays
4 Rigid, pivoted mounting for rear axle attachment point

Figure 10: 1200N Seat Load Case [2]

For the purposes of the Finite Element Analysis (FEA), the rear axle was modeled as being fixed in all directions except for rotation about the axle and the front axle was free only in rotation about the axle and horizontal translation along the axis formed by the line between the two axles. This matches well with the boundary conditions outlined in the test cases above. An example of the FEA results are shown in Figure 11, the others can be found in Appendix A

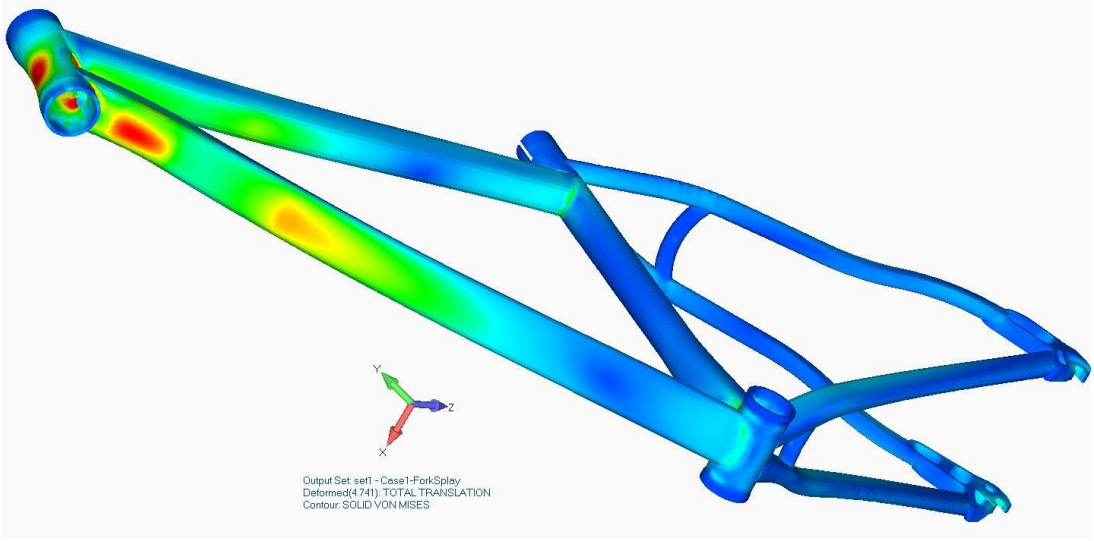

Figure 11: FEA Results of 1200N Fork Splay Simulation

The FEA produced models that could be used to locate strain gauges in areas of high stress concentration.

Using the results of the FEA, 5 strain gauge rosettes (Figure 12) were installed, which included 3 strain gauges each at angles of 0° and ±45°. The advantage to using rosettes is that they can resolve strain in multiple directions in the same location. This confers the ability to discern different loads at the same point, and to determine the precise direction of the primary strain if needed. The locations of the strain gauges are given in Table 3.

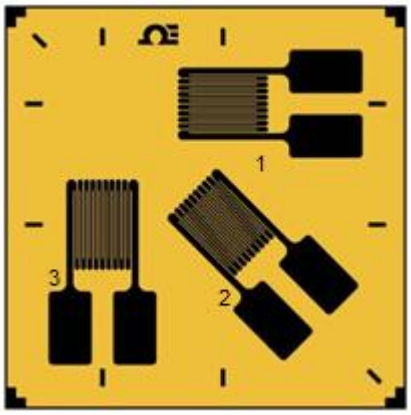

Figure 12: Strain Gauge Rosette

Table 3: Vertex Frame Strain Gauge Layout

Location	Strain Gauge Number	Abbreviated Name
Top face of the top tube, gauge 2 in-line with the tube, 5 cm from the head tube weld.	1	TT_e1
	2	TT_e2
	3	TT_e3
Bottom face of the right chain stay, gauge 2 in-line with the tube, 10 cm from the bottom bracket	1	R_Ch_e1
	2	R_Ch_e2
	3	R_Ch_e3
On the right face of the down tube, gauge 2 in-line with the tube, 10 cm from head tube weld	1	DT_Side_e1
	2	DT_Side_e2
	3	DT_Side_e3
Bottom face of the down tube, gauge 2 in-line with tube, 5 cm from the bottom bracket	1	DT_Bottom_e1
	2	DT_Bottom_e2
	3	DT_Bottom_e3

Left Chain Stay, upper surface, gauge 2 in-line with tube, 5 cm from seat tube weld.	1	L_Ch_e1
	2	L_Ch_e2

3.2.2 Initial Fixture Construction

A test fixture needed to be created that could be used to apply controlled component loads to the bicycle frame. Using this fixture, the stiffness coefficients for each strain gauge under each component load could be developed.

The design concept for this fixture was to replicate the boundary conditions used for the Finite Element analysis as closely as possible. The fixture would also have to be able to apply the desired loads to the frame precisely.

The fixture consisted of two main components, the mounting frame and the loading cage. The mounting block would be used to physically mount the bicycle frame to the fixture while the loading cage would provide a means for applying the specific component loads to the bicycle.

The mounting block used a 5'(1.524m) span of a 6"x8" (152mm x 203mm) I-beam reinforced with ½" (13mm) steel plate. This provided a very rigid base onto which angle-iron supports could be affixed. The rear support was rigidly fixed to the I-beam and included a threaded rod onto which the rear dropouts could be mounted. This provided the constraints seen in the FEA at the rear axle (Figure 13). In order to match the FEA boundary conditions at the front axle, the mount was put on rollers and rails were attached to the I-beam along which the mount could roll smoothly (Figure 15).

The loads were applied through steel rope attached to a lever mechanism (Figure 14). This mechanism was designed such that it was safe and easy to add weight to the frame. The lever mechanism provided a 2:1 mechanical advantage which effectively reduced the amount of weight needed to produce the desired tension in the cables. The level and turnbuckle shown are used for maintaining exact conditions needed to provide the calculated load transfer.

Each component load required its own configuration of levers, pulleys and cables. Figure 15 Figure 19 show these configurations for the Vertex Frame.

Figure 13: Vertex Frame on Mounting Block Fixture

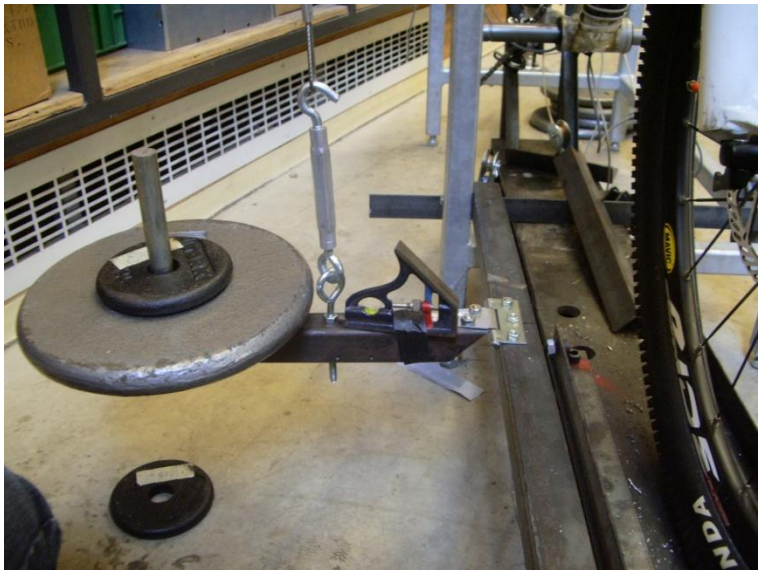

Figure 14: Loading Cage Lever Mechanism

Figure 15: Front Axle Mount and HT MZ Loading Configuration

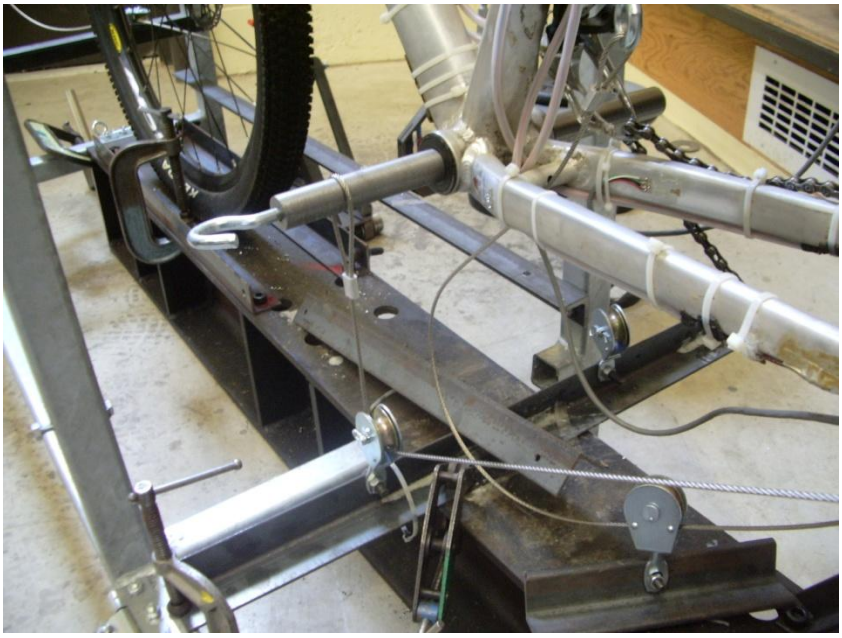

Figure 16: BB MX Loading Configuration

Figure 17: BB FZ Loading Configuration

Figure 18: BB FY Loading Configuration

Figure 19: BB MY Loading Configuration

3.2.3 Stiffness Matrix Development

With the fixture complete, the Vertex frame could be loaded and data collected on the strain reactions.

The first tests carried out were to confirm that the load-strain reaction for all strain gauges would have a linear relationship. This was accomplished by applying incremental loads of 5 lbs from 0 to 300 lbs for each loading direction except for BB FZ, which was limited to 200 lbs for safety reasons, and the brake and chain force, which were omitted during initial testing.

Figure 20 shows a typical result of these tests. The overall results are as hoped, with each reaction being roughly linear. The variance, though, is a concern. The notable steps in the reaction seem to be due to friction within the pulley system of the fixture. This introduces a degree of error into the [k] matrix that could reduce the efficacy of the process.

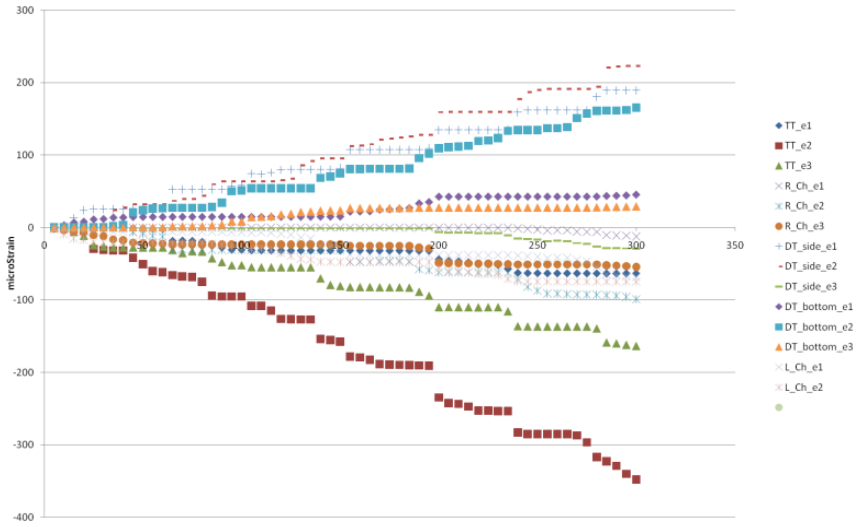

Figure 20: Load in Pounds vs. Microstrain for HT MZ Load

Figure 21 illustrates another concern; the reaction to the BB FY load was so small as to be barely measurable. There was a similar result for the seat load. This is unsurprising as the bicycle frame operates as a nearly perfect truss under these loading conditions, distributing the strain induced by the load very evenly throughout the members of the frame. While this implies that the frame is very sturdy in this loading direction, it introduces the same issue that was encountered with the cantilever beam under compression. It is likely that it will not be possible to get a clean interpolation of the BB FY force through strain readings. N.B. The erroneous DT_side_e1 readings were due to a broken wire that was repaired for later tests.

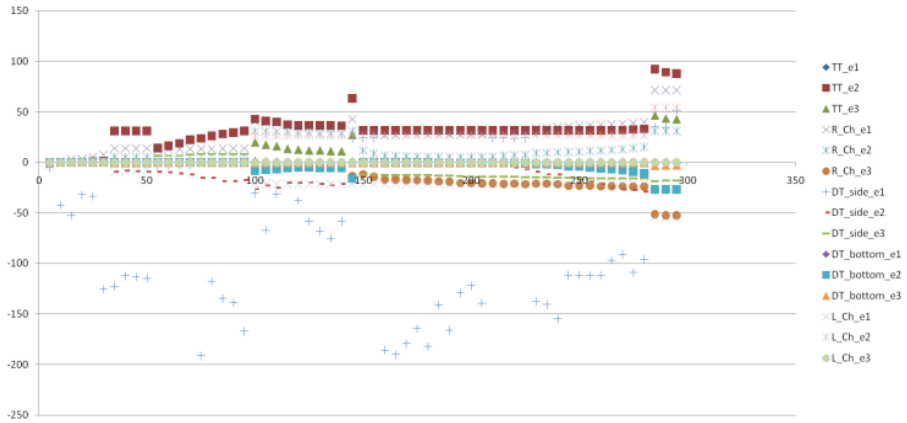

Figure 21: Load in Pounds vs. Microstrain for BB FY Load

The load-to-strain relationships were calculated from the slopes of each line and converted into N/με for component forces and Nm/με for moment loads. The results are tabulated below in Table 4. With the stiffness coefficients known, [j] could be calculated (Table 5: [j] for Vertex Frame)

Table 4: [k] for Vertex Frame

	TT e1	TT e2	TT e3	R Ch e1	R Ch e2	R Ch e3	DT Side e1	DT Side e3	DT Side e1	DT Bottom e1	DT Bottom e2	DT Bottom e3	L CH e1	L CH e2
BB MY	0.848	-0.162	0.157	0.771	1.343	0.786	-1.948	-0.918	-0.079	-1.355	0.348	0.433	-0.285	0.134
BB FZ	0.225	0.006	-0.096	-0.351	-0.647	0.163	0.736	-0.562	-0.171	0.483	0.275	0.129	0.007	-0.001
BB MX	0.848	0.004	-0.191	0.893	1.554	1.397	-1.486	-0.992	-1.505	-0.849	0.434	-0.033	-0.250	0.001
BB FY	0.225	-0.136	0.204	0.037	0.054	-0.013	0.004	0.001	-0.015	0.004	0.007	0.108	-0.052	0.140
HT MX	0.642	0.716	-0.328	0.810	1.367	-0.777	-2.012	4.821	3.570	-1.447	-3.318	-1.838	1.233	-0.733
HT MZ	0.357	1.136	-1.284	-0.053	-0.051	-0.004	-0.120	0.382	0.448	-0.061	-0.080	-0.865	-0.063	-1.079

Units are N/με Cartesian loads and Nm/με

Table 5: [j] for Vertex Frame

	TT e1	TT e2	TT e3	R Ch e1	R Ch e2	R Ch e3	DT Side e1	DT Side e3	DT Side e1	DT Bottom e1	DT Bottom e2	DT Bottom e3	L CH e1	L CH e2
BB MY	0.044	0.016	-0.038	-0.055	-0.110	-0.018	-0.222	-0.362	0.475	-0.258	0.119	0.232	0.142	-0.011
BB FZ	0.376	-0.341	-0.130	-0.372	-0.791	1.477	0.065	-0.481	0.510	0.023	-0.773	-0.078	0.419	0.098
BB MX	0.045	-0.076	-0.027	0.055	0.078	0.432	0.047	0.139	-0.396	0.122	-0.245	-0.221	0.013	0.027
BB FY	2.063	-0.674	1.204	-0.427	-0.482	-0.162	-0.131	1.646	-0.367	0.801	-0.332	-0.556	-6.130	-0.184
HT MX	0.031	-0.078	0.002	-0.034	-0.084	0.259	-0.021	0.031	0.079	-0.007	-0.212	-0.054	0.092	0.032
HT MZ	0.322	0.291	-0.142	0.025	0.095	-0.411	0.020	0.108	-0.016	0.051	0.302	-0.086	-0.503	-0.246

Units are N/με Cartesian loads and Nm/με

3.3 Data Collection and Processing

The strain data was collected on a National Instruments cRio 9014. The cRio is equipped to sample twenty-four channels simultaneously, of which fourteen were used for the initial tests with the Vertex frame. The channels were sampled at a rate of one kilohertz as raw voltage in binary format.

RMB provided the research team with software to convert the binary data from the cRio to floating point values. MatLab code was then developed to process the raw voltage into applied loads and to provide visualizations. The process implemented is as follows:

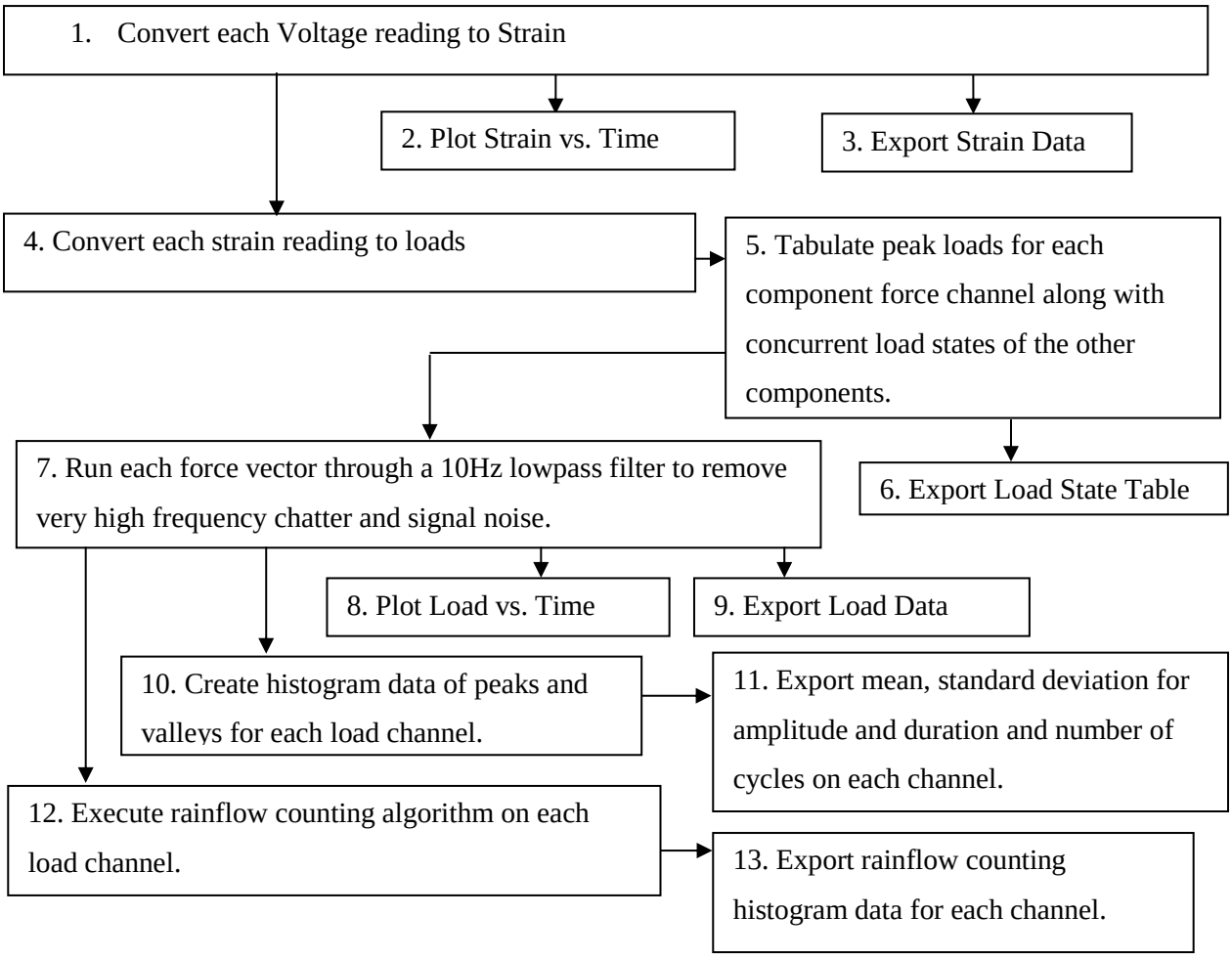

1. In order to convert each voltage reading(V) in the raw data to strain (ε), a quarter bridge (Figure 22) conversion equation is employed (eq. 9) where G_f is the gain factor for the strain gauge (2), R_L is the resistance of the leads (≈0Ω) and R_3 is value of the resistors in the bridge (120Ω). This formula is applied individually to each voltage reading.

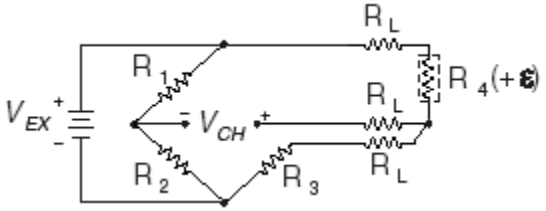

Figure 22: Quarter Bridge Strain Gauge Circuit [24]

$$\varepsilon = \frac{-4V}{G_f(1+2V)} + \quad 1 + \frac{R_L}{R_3} \quad \text{eq. 9 [24]}$$

2. The strain data is plotted with respect to time as a line graph. A sample plot is shown in Figure 23.

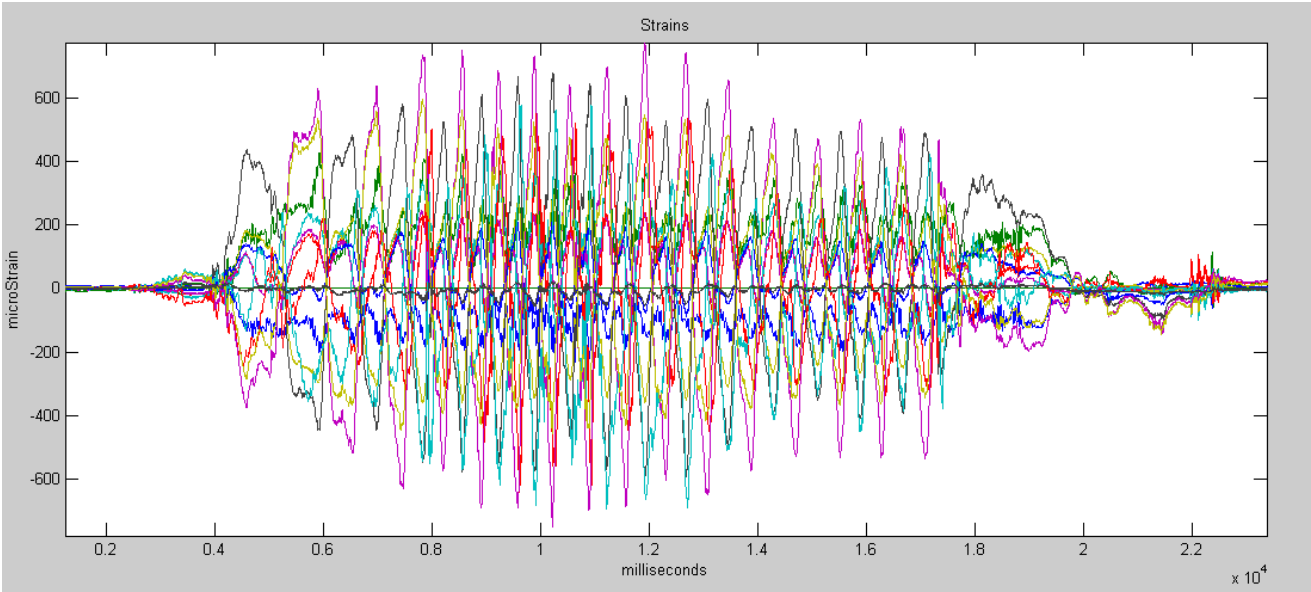

Figure 23: Twenty Second Hill Climb Strain Data on Vertex Frame

3. The strain data is exported in a comma separated value format (csv). Each column represents a strain gauge and each row represents a single sample. Again, the data acquisition unit is running at one kilosamples per second

4. Each row in the strain data is converted into a vector of forces using eq. 8. The forces are in the units of Newtons for linear component forces and Newton-meters for bending moments.

$$P = k^T k^{-1} k^T \epsilon \quad \text{eq. 8}$$

5. For the purposes of investigating peak loads on the frame, the maximum load in both the positive and negative direction is found for each force and all of the loads on the bike at that moment are recorded and tabulated. Examples from sample rides are shown in Table 6: Sample Maximum Negative Load States and Table 7: Sample Maximum Positive Load States

Table 6: Sample Maximum Negative Load States

	HT MZ	BB MX	HT MX	BB MY	BB FZ	BB FY
HT MZ	-100.1	-23	-17.54	28.68	-17.22	-49.91

BB MX	117.1	-257.86	285.7	-96.16	-210.65	237.69
HT MX	92.63	-172.53	-147.28	-149.42	-130.05	-734.35
BB MY	115.22	-166.07	-140.07	-154.52	-105.01	-729.81
BB FZ	30.74	80.24	-47.79	75.36	-692.22	2286.72
BB FY	39.13	112.37	-43.58	49.47	-531.2	-2425.4

Units are in Newtons for Cartesian loads and Newton-Meters for Moment loads

Table 7: Sample Maximum Positive Load States

	HT MZ	BB MX	HT MX	BB MY	BB FZ	BB FY
HT MZ	250.04	-63.78	-12.2	35.09	-51.55	70.77
BB MX	6.09	132.7	-38.76	-8.11	-404.06	2173.3
HT MX	115.28	-257.38	286.08	-95.6	-209.88	235.45
BB MY	31.72	78.73	-47.78	75.48	-690.81	2188.85
BB FZ	52.16	103.07	-73.29	27.49	948.27	-1870.35
BB FY	29.28	82.13	-44.73	68.75	-631.19	2586.15

Units are in Newtons for Cartesian loads and Newton-Meters for Moment loads

6. The maximum load state tables are exported as csv files
7. Each force channel is run through a 10 Hz low-pass filter. This effectively removes high frequency chatter from the terrain and smoothes out signal noise while keeping the larger terrain effects and rider effects represented. The value of 10 Hz was determined through inspection of the Fourier plot of several sections of various rides (Figure 24). The significant peaks fell on the range of 1 to 7 Hz so 10 Hz was selected as a safe cutoff.

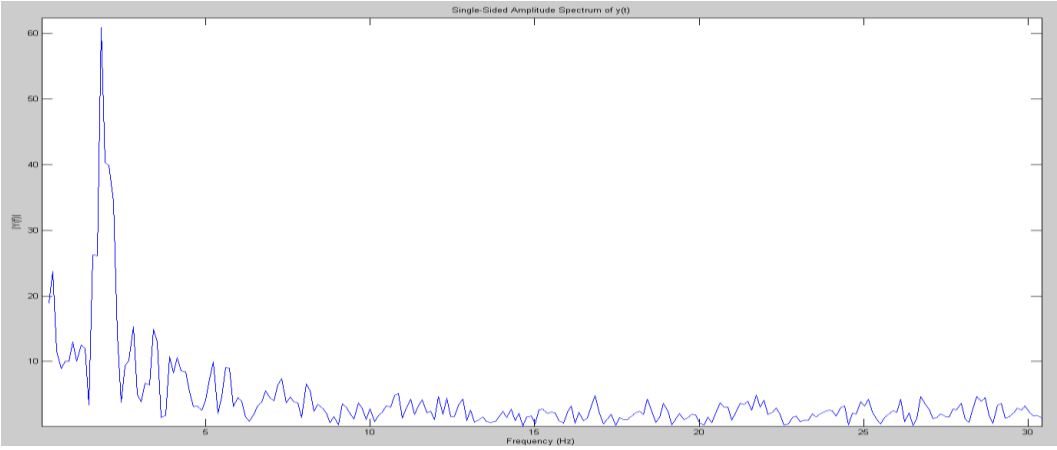

Figure 24: Example Frequency Domain Plot of Strain Due to Pedaling

8. The filtered load data is plotted. A sample plot is shown below in Figure 25.

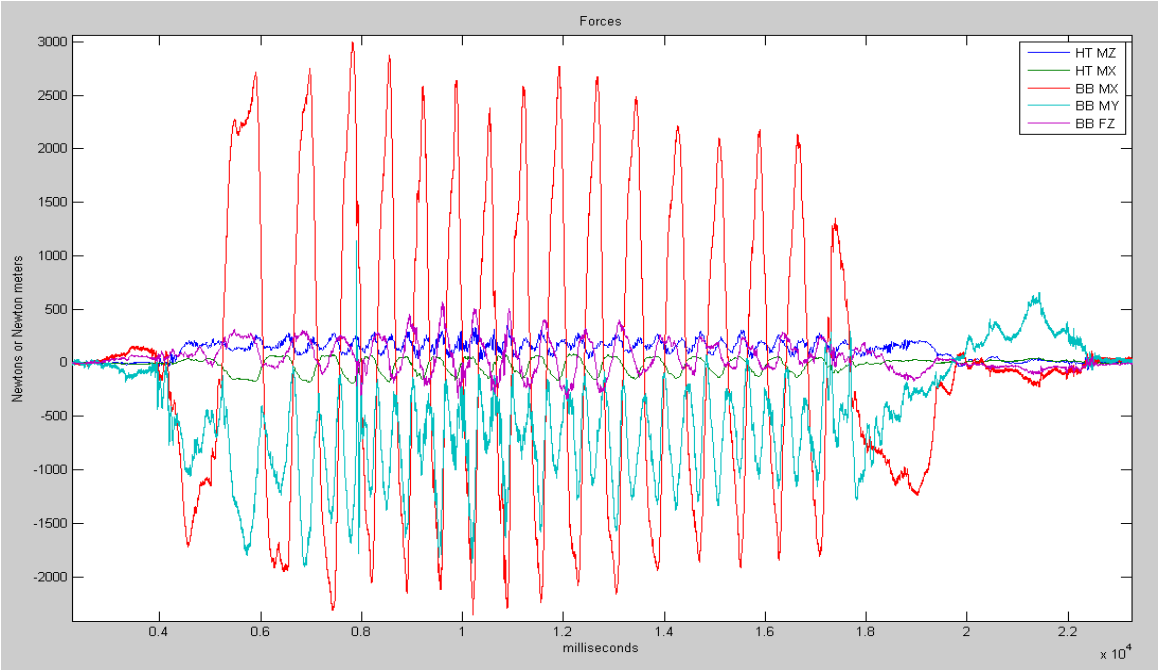

Figure 25: 20 Second Hill Climb Force Interpolation on Vertex Frame

9. The load data is exported as a csv file.
10. Histogram data is collected for each load channel. This is done by calculating and recording the median load and counting the number of times the load crosses the mean, the time between each crossing, the and the peak value reached.
11. A summary table is exported from the histogram data including the peak and mean values, and standard deviation. An example table is shown in Table 8.

Table 8: Summary of Statistical Data of a Sample Ride

	HT MZ	BB MX	HT MX	BB MY	BB FZ	BB FY
Median magnitude	44.9 Nm	-1.31 Nm	-15.21 Nm	-17.04 Nm	-50 N	-7.67 N
Number of peaks	622	685	797	660	761	935
Number of valleys	622	686	798	661	762	936
Mean Positive Amplitude	31.89 Nm	49.57 Nm	48.92 Nm	23.43 Nm	127.79 N	337.37 N
Mean Negative Amplitude	-30.84 Nm	-82.12 Nm	-35.54 Nm	-41.88 Nm	-112.81 N	-357.2 N
Standard Deviation of Positive Magnitude	25.2 Nm	73.28 Nm	69.6 Nm	26.33 Nm	208.05 N	792.36 N

Standard Deviation of Negative Magnitude	27.59 Nm	65.17 Nm	35.76 Nm	39.59 Nm	119.48 N	506.99 N
Mean Positive Duration	319.25 ms	286.78 ms	249.05 ms	300.84 ms	259.07 ms	212.17 ms
Mean Negative Duration	313.06 ms	289.47 ms	248.84 ms	300.42 ms	260.6 ms	212.15 ms
Standard Deviation of Positive Duration	374.48 ms	383.16 ms	263.46 ms	418.37 ms	343.5 ms	188.56 ms
Standard Deviation of Negative Duration	449.81 ms	242.04 ms	221.55 ms	256 ms	271.1 ms	178.06 ms
Peak Positive Load	219.45 Nm	1570.6 Nm	449.2 Nm	484.73 Nm	2839.56 N	19402.14 N
Peak Negative Load	-141.59 Nm	-408.56 Nm	-316.18 Nm	-187.25 Nm	-1299.83 N	-3873.16 N

12. Each load channel was processed using the rainflow counting algorithm created for MatLab [25] following the ASTM standard practices for cycle counting in fatigue analysis. The cycles were counted based on amplitude and offset from the mean, yielding a two dimensional table of cycle counts. Table 9 shows a section of the histogram data for a sample ride. The full table has thirty bins in each direction and is too large to display here.

13. The rainflow histogram data are exported for each load as csv files.

Table 9: Sample Rainflow Counting Histogram Data for HT MX during 3 Minute Ride

		Cycle Load (Nm)							
		6	**19**	**32**	**45**	**57**	**70**	**83**	**96**
Offset from 0 (Nm)	**-99**	3	0	1	0	0	0	0	0
	-87	4	1	1	0	0	1	2	0
	-75	6	2	0	1	1	1	1	0
	-63	10	3	1	4	3	1	0.5	0
	-51	29	10	8	12	2	1	0	1
	-39	73	41	40.5	16	2	5	0	0
	-28	149	95	32.5	5.5	2	1	0	1
	-16	360	74	9	5	4	7	1	2
	-4	214	5	13	3	7	1	1	3
	8	20	11	9	5	7	4	1	1
	20	5	1	6	9	4	0	4.5	3
	32	7	3	3	2	9	8	1	3
	44	8	6	2	3	3	6	7	4
	56	6	1	1	0	1	1	5	6
	68	4	1	2	0	0	0	0	0

3.3.1 Initial Field Trials and Results

With the [j] constructed it was then possible to test the system in ride scenarios. The initial test rides were designed to be as short and repeatable as possible. The first tests were carried out at very low speeds on a flat concrete floor. This Made it possible to count the number of rotations of the pedals, control gearing and braking, and ignore most effect of surface induced vibration. If the system can be shown to be effective in this environment then it would be ready for field trials on natural terrain.

The plots in Figure 26 to Figure 29 show the results of four of the short tests that were carried out indoors. Note that the loads were calculated in pounds for these tests as it was easier to compare the results to the loads applied to the test fixture.

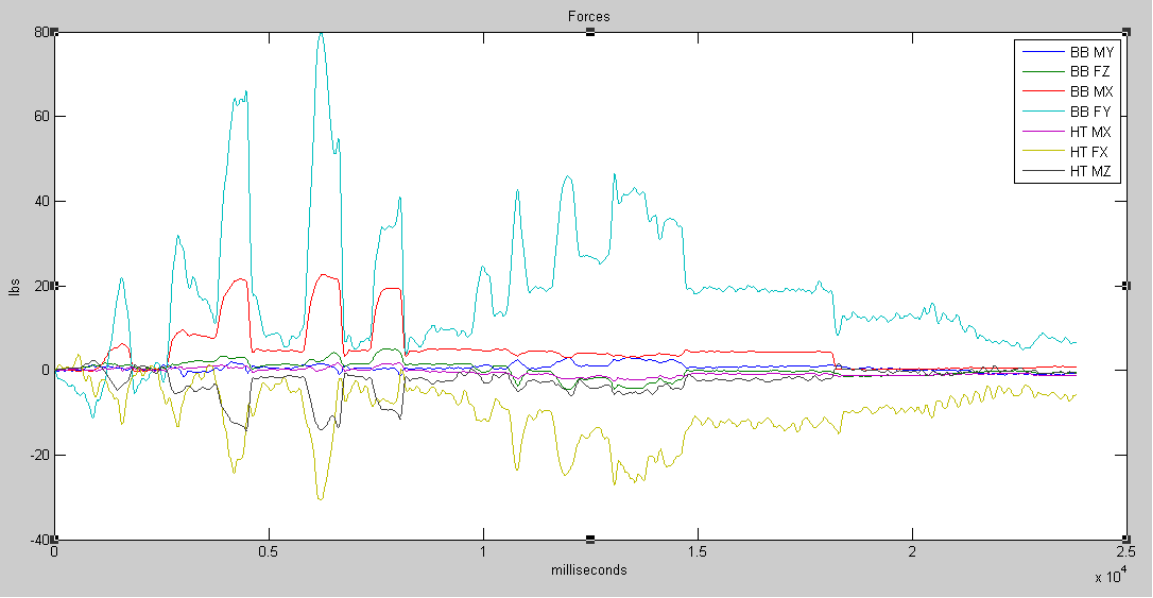

Figure 26: Changing Gears While Standing on Flat Ground

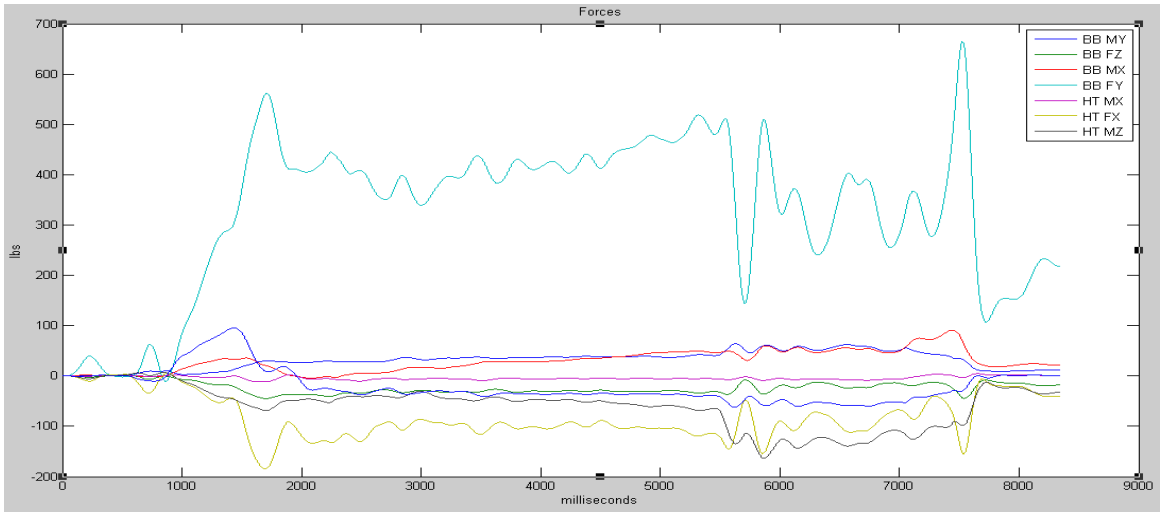

Figure 27: Engaging Rear Brake after Short Descent on Ramp

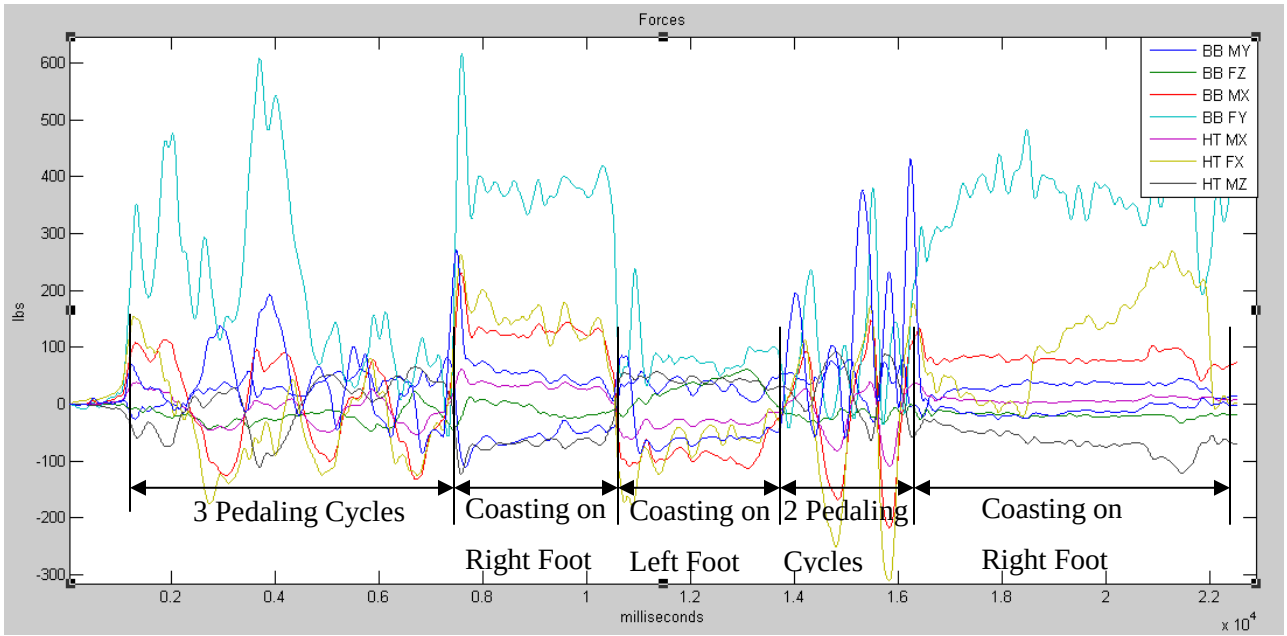

Figure 28: Pedaling Along a Corridor

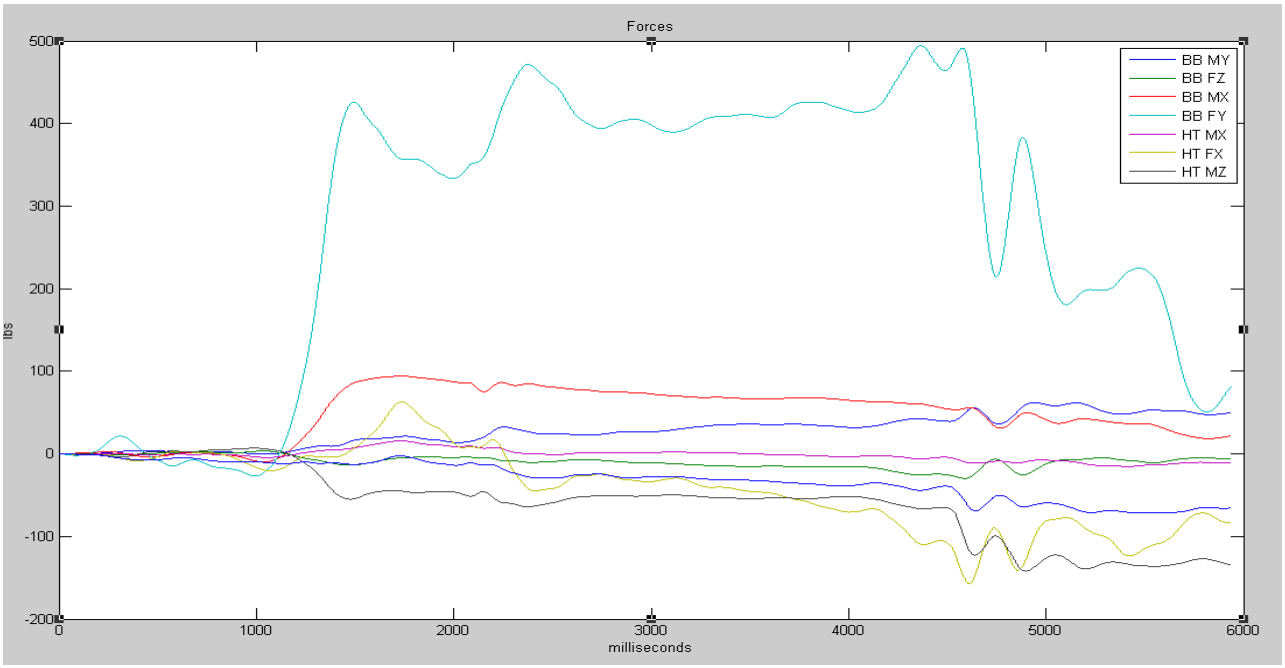

Figure 29: Engaging Front Brake after Short Decent on Ramp

The tests were positive overall and yielded what seemed to be reasonable results except for the BB FY force. It was much larger and more variable than it should be. Previous research [19] indicated that this force should vary between half and twice rider weight under normal conditions. Because of this force being clearly erroneous it is omitted from further figures in this section so as to make the other loads more readable.

The next exercise was to test the system under field conditions. A series of tests were done at McClennan Stunt Park in Kitchener, Ontario (Figure 30). This provided an environment for short, repeatable tests in a setting somewhat analogous to actual trail riding while still being short enough to monitor the details of the ride such as braking and pedal counts.

Figure 30: McLennan Park

The first set of tests run was simple climbs up the steep incline. Figure 31 shows a typical result. Note that the moment about the bottom bracket dominates the loads being applied. This was found to be a typical result. A second rider was employed on the same test to compare the effects on the measured loads (Figure 32). It was found that the peak loads increased in the same ratio as the rider weight.

One surprising result was the BB MY, which was expected to be quite small and to be roughly sinusoidal centered on zero. This was an indication that at least one significant load was acting on the system that had not been incorporated into the development of [k].

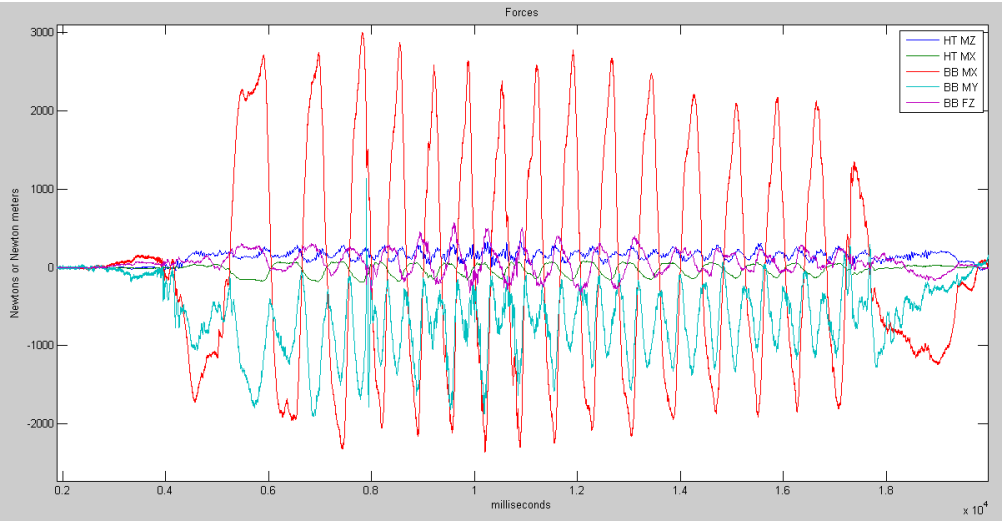

Figure 31: Steep Incline Climb McLennan Park 70 kg Rider

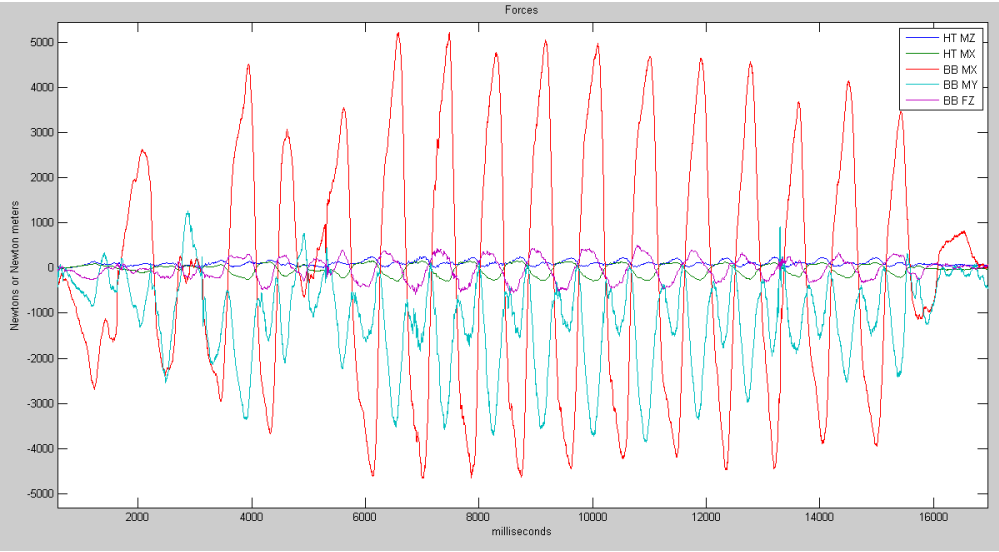

Figure 32: Steep Incline Climb at McLennan Park 100 kg Rider

The second set of tests involved the same riders coasting down a slope with three small jumps made from hard-packed dirt (Figure 33). While there were similar concerns as to the validity of the data as with the climbing, the fact that the overall magnitude of the loads was significantly less for what might be considered more aggressive and high-impact riding was surprising. Closer inspection

of the strain data, though, verified that this was, in fact, the case. It seems that the geometry of the frame deals very well with jumping and landing as long as they are clean and well balanced maneuvers. The primary load would be on the handlebars and bottom bracket, which, as discussed before, spreads strain through the frame very evenly

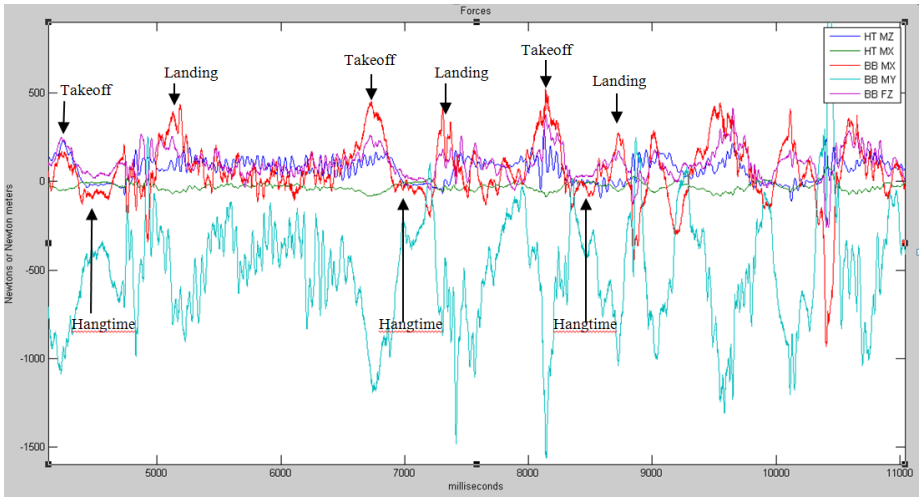

Figure 33: Loads from 3 Small Jumps While Coasting Down a Hill

An even clearer picture of the relative loads to pedaling and landing jumps can be seen in Figure 34 where a rider jumped off of a 2m drop-off and landed on a slope.

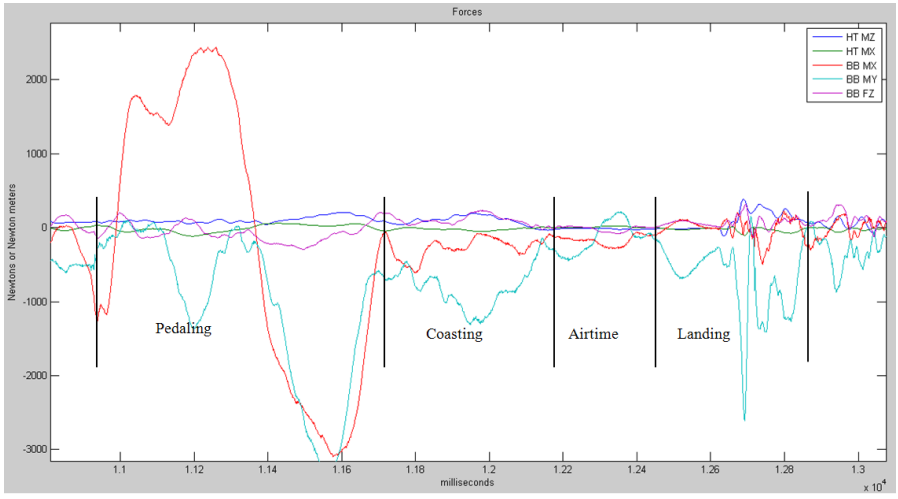

Figure 34: Loads from 2m Drop-off

3.3.2 Error Estimation

The field tests indicated that the system, as it existed, was not providing accurate results. There were two primary concerns. First was that it was unclear what precision could be expected from the use of [j] matrix method. The second was whether any key forces were missing from the construction of [k].

In order to investigate the expected precision of [j] matrix, a Monte Carlo simulation was created. The purpose of this simulation was to compare the loads predicted by the [j] matrix that were experimentally determined to those that would be predicted by other possible [j] matrices that could have been generated based on the variance in the measurements found during the creation of the [k] matrix.

The process for this was to take a sample ride and process each sample both using the actual [j] matrix and then processing the same sample using a [j] matrix constructed by altering each value in the original [k] by a small amount based on a normal distribution with a variance defined by measurements in the original construction of [k].

The results of this analysis were somewhat disappointing. The predicted errors were all found to follow an exponential distribution closely with mean values listed below (Table 10). The loads at the head tube were very precise, by this analysis, but the moments at the bottom bracket varied unacceptably and the BB FY load was completely unusable as the error is on the same order as the weight of the rider.

Table 10: Expected Error for Initial Vertex [j]

	Mean Error	Mean % Error
HT MZ	11 Nm	0.8
HT MX	22 Nm	1.5
BB MX	1010 Nm	73
BB MY	673 Nm	45
BB FZ	198 N	13
BB FY	573 N	276

Inspection of [k] gave some insight into why some component forces were more reliably precise than others. HT MZ and HT MX each had a single strain gauge that provided a strong reaction to those loads but did not react very strongly to the others while BB MX and MY had gauges that reacted similarly to each other. This small difference between the strain reactions made the matrix very sensitive to error.

BB FY did not have any gauges that reacted strongly to that component load. This, as noted before, is expected given the geometry of the frame. However it does produce a challenge when attempting to interpret that load.

Determining if there were important forces being omitted is difficult to determine from the data gathered thus far. The only apparent means of testing this issue is to repeat the entire process, this time including all possible component forces.

3.4 Areas of Improvement

The previous work on the RMB Vertex frame produced encouraging results, but with some clear areas in need of investigation and development. Through inspection of the data, it became clear that the strain gauges could be better located. It also became apparent that some significant component loads may not have been represented in the initial construction of the matrix. Careful comparisons between ride conditions and the test fixture also indicated that the boundary conditions used in the FEA, upon which the fixture was based, do not reflect those of actual riding well for all loading scenarios. Finally, precision in the construction of the [k] matrix was found to be critical as the expected error in the system was very strongly affected by the accuracy of [k].

3.4.1 Improved Strain Gauge Locating Protocol

Thorough inspection was carried out on the [k] matrix of both the Vertex frame and the cantilever aluminum tube in order to determine any patterns by which the locating of gauges could be improved. The original criterion was that the gauge be located on an area that showed high strain in FEA. Investigation, though, showed that the process would need to be more nuanced. The following constraints all needed to be met to make a location suitable:

1. Location must have a high strain-to-load ratio (>1με/5N) for at least one load case
2. Location must have a unique strain-to-load ratio for at least one load case
3. Location must be on a smooth, exterior, non-welded location
4. Location must be at least 5cm from any moving mechanical part
5. Location must be unlikely to be hit by debris or the rider during riding

The first requirement, of having a high strain-to-load ratio, is based on the results of the cantilever pipe and Vertex frame tests. The reaction of one micro-strain per five Newtons of load produced a strong enough signal to interpret the loads. A consequence of this criterion is that if there

is no location on a frame with a high load-to-strain ratio for a given component force, that load cannot be meaningfully resolved.

The second requirement was developed through some trial and error. It was found that there was a location on the down tube near the head tube that had a strong reaction to all loads that were applied. This location turned out to be of no value because even though the reaction was clear and measurable, it could not be used to differentiate between loads.

The third requirement is due to the limitations of strain gauge application. They require smooth surfaces with little curvature in order to adhere well and give meaningful measurements.

The fourth requirement was determined after some strain gauges were placed close to sprockets and pedals. These gauges seemed to pick up extra noise in the signal and were therefore less precise in their measurements.

The final requirement is simply a consideration for durability. Strain gauges are not particularly tough or resilient to damage from impact or abrasion. Even though the gauges are to be protected with a resin coating and a rubber barrier, it seemed prudent to keep them out of the areas of the frame most likely to be hit or rubbed against while riding.

3.4.2 Considerations for Omitted Loads

It was noted that the BB MY loads in the Vertex trials was unexpectedly large. This is most likely a consequence of not including some important component loads in the analysis. The tension in the chain is likely to have been a major contributor to the unusual results in BB MY.

This then, indicates that the method is not useful for investigating only a couple loads of interest. If the [k] matrix does not include all significant loads, the [j] matrix will give erroneous results as it fits the measured strains to the loads available as best it can.

3.4.3 Boundary Conditions for FEA and Test Fixture

The boundary conditions and mounting techniques used in the standardized test for mountain bicycle strength [2] were a good starting point for testing; however those tests combine or omit a variety of loads. For example, standard test for pedaling combines the chain, BB MX, BB MY, BB FZ and BB FY forces. In order to separate these loads and measure them in a way that they could be meaningfully resolved separately, a more complex mounting system would be needed. The following is a list of requirements for accommodating all of the meaningful loads on the frame.

1. The head tube needs to rotate freely in all directions relative to a fixed rear axle. It is also possible to fix HT MX direction and have the rear axle free; the effect is mathematically the same.
2. It must be possible to load the head tube in the MX and MZ directions to simulate fork splay and a relative twist between the front and rear axle.
3. The rear axle needs to be able to rotate freely in the MY and MZ direction to simulate a free spinning axle and the wheel rotating about its contact point with the ground surface.
4. The bottom bracket must be able to be loaded in the FY, FZ, MX and MY directions independently.
5. It must be possible to simulate a pure chain load.
6. It must be possible to simulate a pure rear brake load.

3.4.4 Precision in [k] development

It was found that a major contributor to the expected error in the system was the precision with which the loads were applied to the frame in the initial testing. The fixture introduced some friction through the pulley system being used meaning that the actual load being delivered to the bicycle frame.

A new fixture should have the capacity to measure loads being applied at the connection point to the frame.

Chapter 4
Final Implementation

4.1 Redesign of the Fixture

With the considerations noted in section 3.4.3 the loading fixture was redesigned. In addition to the listed requirements, there was the additional need to be able to accommodate other bicycle frames that may be involved in future research.

The new fixture was designed to use much of the material from the original, along with extruded aluminum framing that was available. Cost was a major concern in the development of this fixture so much of the work was done with inexpensive or retrofitted components. The focus on the rebuild was precision for static loading for which aesthetic considerations and ease of use were largely sacrificed.

The mounting of the head tube was altered considerably. The original design (Figure 15) had the front forks attached to a sliding block. This was entirely replaced by a three axis gimbal mechanism that allows rotational movement about the centre of the heat tube but no translational movement at all (Figure 35,Figure 36). This was equipped with an extended lever arm in the form of a 1½" UNF threaded rod on which the HT MX and MZ torsional loads could be applied.

Figure 35: Head Tube Mounting Gimbal, Empty

Figure 36: Head Tube Mounting Gimbal, Loaded with Element Frame

The rear mounting block was altered to allow for translation in-line with the frame. This provided both the freedom needed to simulate the freedom of the bicycle frames to deflect in this direction as well as a means to adjust for bicycle frames of different sizes. It was also equipped with a system of sturdy bearings which allowed rotation about the y-axis while remaining rigid in response to other loads (Figure 37).

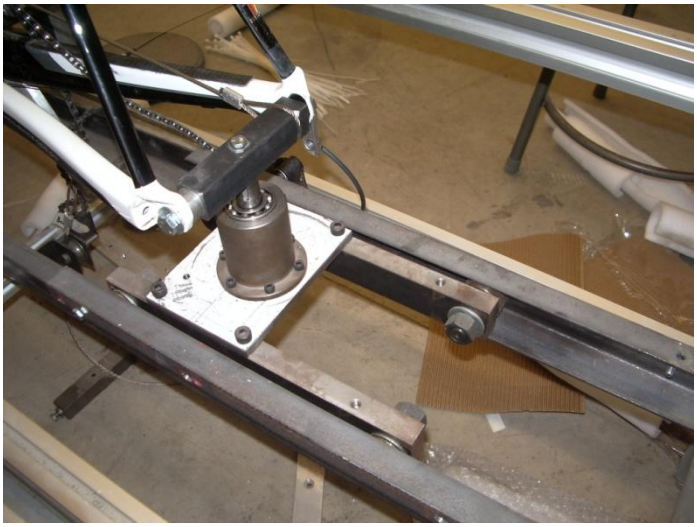

Figure 37: Rear Dropout Mounting Fixture

In order to replicate rear brake forces, custom hardware needed to be made for each type of brake. The hub-mounted disk brakes were replicated using an aluminum lever arm which attached to the axle and the brake mounting points on the frame (Figure 38). Rim brakes required a small, relatively rigid plate to attach to the frame at the point where the calipers would mount (Figure 39)

Figure 38: Rear Disk Brake Loading Arm

Figure 39: Rim Brake Load Mounting Plate

The bottom bracket forces were applied using cables attached to a solid steel bar with the same diameter as the crank arm axle, inserted through the bottom bracket bearings (Figure 40).

Figure 40: Bottom Bracket Loading Arm

The chain force was replicated by attaching a lever arm to the steel bar being used to apply loads to the bottom bracket and connecting that arm to the rear axle (Figure 41)

Figure 41: Chain Load Lever Arm

The whole fixture was assembled around extruded aluminum framing which allowed for exact positioning of the loading levers (Figure 14) and pulleys and accommodated any size of frame that might be loaded on the fixture (Figure 42).

Figure 42: Complete Static Loading Fixture

In order to increase precision of the applied loads, a game scale was attached between the loading cable and the load points on the frame. This provided a precision of better than 10 Newtons which was an order of magnitude improvement over the previous fixture.

4.2 Strain Gauge Application

As explained in section 3.4.1, the locating process for strain gauges on bicycle frames needed to be changed. The first step in this was to change the boundary and loading conditions of the FEM to match the alterations to the test fixture. The easiest way to do this was to create simplified rigid analogues of the mounting and loading units themselves. Once properly constrained, the FEA was carried out using a unit load for each component force (Appendix A)

The FEA strain mapping was used to locate all of the locations of strain concentrations on the physical frames themselves using coloured stickers to discern between loads (Figure 43). This mapping of on the frame helps locate potential locations for strain gauges which can then be filtered using the criteria listed in Section 3.4.1.

Figure 43: Strain Concentration Locations for Various Loads

With the specific locations determined for each frame, the surface paint was removed carefully by sanding, leaving the carbon fiber frame exposed. The strain gauges were applied directly to the carbon fiber frame (Figure 44) and leads were attached as shown in Figure 45. The purpose of the double leads on alternate contacts is to balance the resistance through the quarter bridge circuit (Figure 22).

Figure 44: Strain Gauge on Carbon Fiber Frame

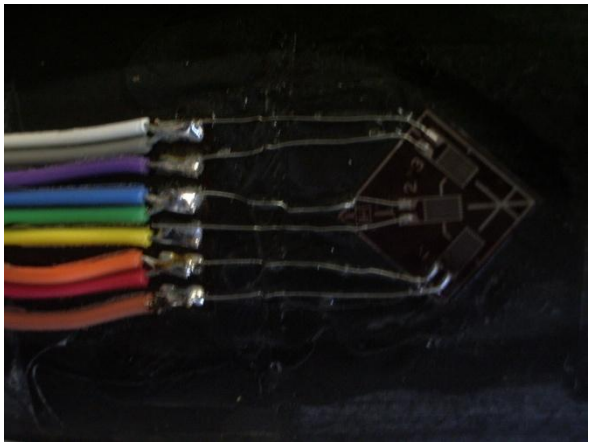

Figure 45: Strain Gauge Leads

4.3 [k] Development

The process for determining the stiffness coefficients for the newly gauged frame is no different than was outlined previously except for the addition of some new component loads and the added precision given by the scale.

An added complication, though, is that the frame in which RMB is most interested, includes rear suspension. The system, as it exists, does not have a means for measuring the travel in the suspension nor adapting to the changes in geometry caused by it. It is possible, however, to estimate the error caused by the suspension by establishing a [k] at the 20% compression level, which is the recommended neutral position when loaded with a rider, and another [k] at the fully compressed level. The results of the force transformations can then be compared

The two completed Matrices are shown below in Table 11 and Table 12.

Table 11: Element K Matrix, Shock at 20% Sag

HT MZ	0.190	-1.320	0.593	-0.694	-1.515	2.591	-0.038	0.954	1.085	1.222	-6.852	-2.668	-1.185	5.591
Seat	-1.096	4.715	-5.540	0.089	4.283	-4.609	-1.029	-4.432	-3.993	-4.600	2.009	-0.380	-4.779	-2.427
Brake	11.461	141.800	13.302	3.268	-5.893	-5.482	-2.227	9.946	7.897	8.319	-1.675	-0.987	10.653	-2.560
BB MX	-0.178	-0.440	0.054	-0.107	-0.199	0.202	-0.375	-0.210	0.056	0.403	-0.047	-0.018	0.527	0.051
HT MX	-3.656	5.966	-3.904	-0.624	2.343	-11.278	-3.980	-6.344	-3.907	-1.820	-0.494	0.634	-3.245	3.469
Crank	2.550	3.075	-51.007	-14.360	11.618	21.685	19.419	-26.937	-15.268	-17.298	-3.743	-0.897	4.160	-8.270
BB MY	-0.164	0.462	2.338	0.628	-0.243	-0.680	-1.003	0.816	0.600	0.979	-0.057	-0.049	0.231	0.063
BB FZ	0.379	-2.455	19.963	6.503	-1.238	-3.916	-1.979	8.682	5.366	5.664	0.016	-0.115	1.233	0.755
BB FY	-0.568	2.507	-1.837	0.139	1.847	-1.289	0.346	-1.623	-1.491	-1.743	0.103	-0.158	-1.938	0.207

Table 12: Element K Matrix, Fully Compressed Shock

HT MZ	0.419	-1.563	0.405	-0.629	3.213	2.499	-0.038	0.938	1.009	1.130	-7.030	-3.103
Seat	-1.072	3.753	-5.262	0.133	-5.250	-4.140	-0.975	-4.225	-3.682	-4.031	1.862	-0.400
Brake	12.169	151.528	11.366	2.509	-1.823	-4.898	-2.169	9.682	7.947	8.352	-0.952	-0.715
BB MX	-0.199	-0.262	-0.134	-0.083	0.096	0.046	-0.328	-0.379	-0.128	0.158	-0.029	-0.062
HT MX	-5.255	8.720	-5.740	-0.821	-15.023	-16.346	-5.856	-9.058	-5.746	-2.730	-0.627	0.723
Crank	3.413	3.255	-50.593	-15.079	11.786	22.871	20.337	-26.343	-15.089	-17.658	-3.636	-1.058
BB MY	-0.129	0.300	2.451	0.714	0.599	-0.671	-0.988	0.880	0.635	0.992	-0.053	-0.057
BB FZ	0.379	-2.455	19.963	6.503	-5.570	-3.916	-1.979	8.682	5.366	5.664	0.016	-0.115
BB FY	-0.573	2.829	-1.886	0.258	-3.009	-1.264	0.485	-1.811	-1.520	-1.594	0.059	-0.168

4.4 Error Estimation

In order to estimate the expected error in the system based on the precision of the [k], the same procedure as was outlined in 3.3.2 was carried out. The results of the Monte Carlo Simulation are shown in Table 13. The improvement over the initial implementation on the Vertex frame is significant. Unfortunately, the precision of [k] is not the only potential source of error.

Table 13: Expected Error based on [k] Precision

Load Direction	Mean % Error	Mean Error
HT MZ	2	8 Nm
Seat	4	50 N
Brake	12	125 N
BB MX	3	13 Nm
HT MX	4	14 Nm
Crank	19	581 N
BB MY	20	29 Nm
BB FZ	10	116 N
BB FY	17	898 N

The element frame, as mentioned previously, has a rear suspension. In order to quantify the error caused by the variations in [k] through these changes, two Monte Carlo simulations were carried out. The first was used to determine the maximum expected error. To do this, data from field trials was processed using both the 20% sag [k] and the fully compressed shock [k] and their results were compared. This, though, is unlikely to be representative of the actual error as very little of the time spent riding involves the rear shock being fully compressed. Without clear data available on the compression level of the rear shock, estimates based on experience were used. The majority of riding seems to keep the rear shock within 10% of the neutral, 20% sag position.

It was also assumed for these purposes that the change in [k] between the two positions would be a linear progression. This seems reasonable as, when comparing the two matrices, there are neither sign changes nor changes in the order of magnitude of the individual strain relations. Thus transitional [k] matrices could be created between 20% sag and full compression based on a linear interpolation between the two. The amount of compression based on the observed shock compression patterns could be modeled using a normal distribution.

This simulation was run in MatLab and again compared to the data processed using only the 20% sag [k]. For each sample, a random compression was generated based on a normal distribution and from that a new [k] was interpolated. The results are shown in Table 14.

Table 14: Expected Error due to Rear Suspension

Load Direction	Max Expected % Error	Expected % Error Based on Normal Distribution	Expected % Error When Combined with Table 13
HT MZ	41	17	19
Seat	92	19	23
Brake	122	35	47
BB MX	161	44	47
HT MX	40	14	18
Crank	71	28	47
BB MY	131	43	63
BB FZ	255	51	61
BB FY	78	15	32

The worst case scenario is, unfortunately, quite bad. However, the predicted mean error based on the normal distribution is, while larger than desirable, still useable. The system as a whole is less precise than is desirable. When the shock error and basic precision error are combined, the results leave the expected error for most component forces near 50%.

This indicates that without an effective method of measuring the shock displacement, this method is useful only for order of magnitude results and determining loading patterns.

Chapter 5
Field Tests

The tests that were performed on the Element Frame before it was returned to RMB for their own interests, focused on the effect of rider weight on the forces experienced during off-road trail riding. Three volunteers from King Street Cycles in Waterloo offered to help in this endeavor.

They were each of significantly different weight, but all were experienced mountain bikers with good knowledge of the trails. Their similar abilities and experience on the trail meant that effects other than biometrics were largely controlled for. Their size and weight were recorded and are presented in Table 15.

Table 15: Test Rider Vitals

Rider	Weight	Height
Rider A	70 kg	176 cm
Rider B	84 kg	183 cm
Rider C	104 kg	190 cm

The trails used were on the Waterloo Hydrocut trail system [26]. The course run was a 1.42 km and included the trails called Kaitlyn's Switchbacks and Rockin' Ronnie. This short loop was chosen for several reasons: it was very familiar to the riders, this improved their ability to take the course at speed safely; it was short enough that it could be done several times by each rider over the course of a day without significant concerns about the effects of exhaustion; and it had a good variety of terrain which was thought to be representative of most features that would commonly be encountered including a variety of rocky, natural and constructed surfaces, steep climbs and descents, sharp turns, substantial obstructions and small drops (Figure 46Figure 52).

Figure 46: Caitlyn's Switchbacks Trail Section

Figure 47: Caitlyn's Switchbacks Trail Section

Figure 48: Caitlyn's Switchbacks Trail Section

Figure 49: Rockin’ Ronnie Trail Section

Figure 50: Rockin' Ronnie Trail Rock Feature

Figure 51: Rockin' Ronnie Trail Rock Feature

Figure 52: Rockin' Ronnie Trail Lock Feature

Chapter 6
Results of Field Tests

6.1 Peak Load Cases

An area of interest for bicycle frame development is the peak loads that the frame is likely to encounter during normal riding. While bicycles must be designed to survive moderate impacts from accidents and crashes [2], the peak forces experienced during normal riding are needed to determine how well a frame will distribute those loads and how it will deflect under non-catastrophic conditions.

To this end, tables were constructed from each ride that indicate the peak load for each component force, as well as the loads on each other force at that point. An example of this table is shown in Table 16 and**Error! Reference source not found.**

Table 16: Max Forces for Rider 1 on Kaitlin's Switchbacks and Rockin Ronnie

	HT MZ	Seat	Brake	BB MX	HT MX	Crank	BB MY	BB FZ	BB FY
HT MZ	**273**	-86.75	84.57	-63	-37.55	191.38	47.36	-65.42	-108.23
Seat	183.91	**209.91**	250.53	-126.8	112.55	671.38	-92.06	-85.26	-237.69
Brake	-3.77	-306.65	**1570.6**	74.78	-28.96	-774.05	-0.72	-21.84	781.79
BB MX	46.03	3.93	73.39	**145.82**	-58.7	2563.48	-17.31	-420.41	-2152.23
HT MX	33.23	4.59	-425.91	-247.75	**382.55**	4097.28	-35.23	-283.98	-84.04
Crank	98.3	-209.66	-720.79	-245.7	-15.81	**6196.93**	107.02	-118.74	15.61
BB MY	-202.04	-312.84	519.06	-206.94	-1.02	1799.39	**152.51**	-16.16	58.7
BB FZ	15.43	-777.87	124.9	-13.08	-85.28	514.09	42.42	**468.65**	-178
BB FY	33.96	-1418.73	47.78	32.17	-19.3	751.3	28.89	-275.72	**1911.55**

Table 17: Min Forces for Rider 1 on Kaitlin's Switchbacks and Rockin Ronnie

	HT MZ	Seat	Brake	BB MX	HT MX	Crank	BB MY	BB FZ	BB FY
HT MZ	**-227.14**	-611.77	815.35	-225.01	66.84	1631.39	139.93	-58.84	49.61
Seat	100.94	**-2291.01**	209.36	-169.86	-143.28	836.48	-154.02	-109.17	-1185.31
Brake	99.48	-198.54	**-720.91**	-246.17	-15.13	6195.01	107.3	-117.98	11.63
BB MX	73.49	-857.77	-30.36	**-334.81**	377.88	1596.19	-111.11	-267.17	211.29
HT MX	102.81	-43.2	-355.71	-228.11	**-239.61**	4173.38	-110.19	-163.04	-515.14
Crank	-3.82	-308.06	1566.36	78.85	-31.79	**-780.22**	1.02	-20.44	680.29
BB MY	151.13	-634.5	483.9	-248.85	-201.15	1641.3	**-212.92**	-153.02	-1271.12
BB FZ	121.82	-37.93	-15.93	-54.77	211.74	352.3	14.04	**-778.62**	-921.33
BB FY	41.34	-674.59	906.41	97.13	-56.86	-228.02	18.13	55.01	**-2742.39**

The value of this tool is primarily for validating designs under specific conditions. A designer can run a chosen rider through a desired course and use those results to investigate how a new frame would manage specific load conditions on that course.

6.2 Rider Weight Model

With the results from the three riders it was possible to verify the findings of Stone and Hull in that the relationship between rider weight and applied load was linear [19]. To do this, the maximum, minimum, and median values for each load on each test were found. In addition, the mean value for the local maxima and minima were found for each, giving a reasonable expected value for cyclic loading.

Given that there were only seven tests with three riders, the results are remarkably consistent. Almost all forces show a clear linear relationship with weight with an extrapolated intercept near the origin. See Appendix B for the calculations and individual results.

There were two clear exceptions to the linear trend. The first is the BB FY force, which is very much expected to follow a linear relationship. However, due to the known inaccuracies in that loading direction, it is not possible to draw meaningful conclusions from the data. The second is the BB FZ direction. This direction showed no clear relationship between rider weight and load, which was surprising but there is a mechanism by which it might be explained.

The BB FZ direction can only be loaded if the frame is tipped relative to the rider such that the forces that are being applied to the pedal are out of the plane of the frame. This effect is more related to riding style and possible terrain effects rather than weight.

6.2.1 Model Compared to Standard Testing

The linear model for mean and extreme loads calculated from the field tests can be compared to the standard fatigue test loads (

Table 18) for bicycle frames to help determine at what weight those tests are most valid [2].

Table 18: CEN Fatigue Test Loads

	+	-
HT MZ	550	-270
Seat	0	1200
Brake	-	-
BB MX	200	200
HT MX	-	-
Crank	1980	0
BB MY	20	-20
BB FZ	160	-160
BB FY	0	1200

The BB MY load is fairly clearly under-represented in the standardized tests. Figure 53 shows the comparison between the modeled load response and the standardized test loads. Any rider much more than 70 kg will be exceeding the tested level frequently for the majority of their pedal cycles, and there appears to be no weight at which the peak loads experienced in this direction will not vastly exceed the required testing.

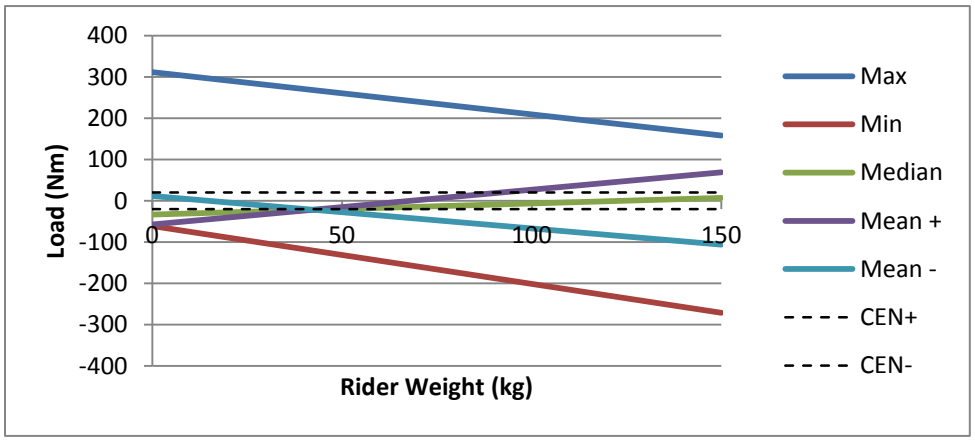

Figure 53: BB MY Modeled Weight Response and Standardized Test Levels

The BB FZ direction (Figure 54), despite not having a clear rider weight relationship, does seem fairly well represented by the standard tests. The mean loads for all the tested riders stay roughly within the range of the fatigue testing. However, the peak loads, again, exceed these limits considerably and should, perhaps be considered explicitly in design.

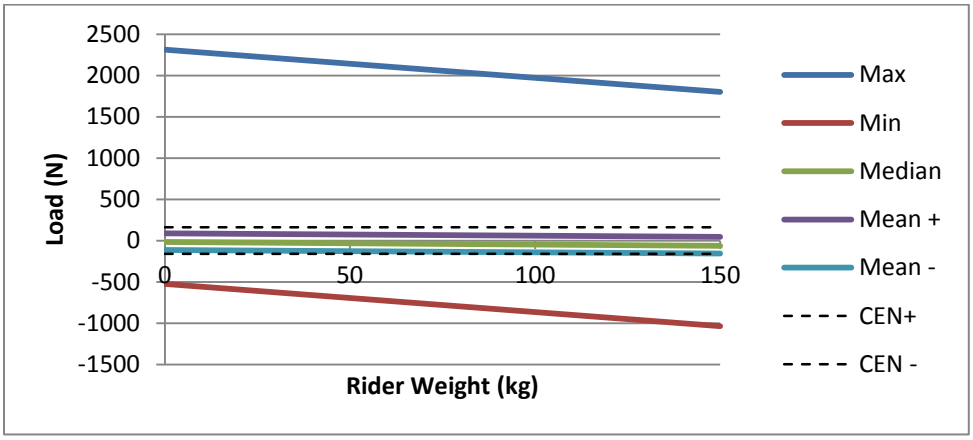

Figure 54: BB FZ Modeled Weight Response and Standardized Test Levels

In the case of the load transferred through the chain, the standardized tests also seem reasonable (Figure 55). While the maximum loads seen in this direction exceed the fatigue test load, the expected loads stay well below that level until the rider crosses 100 kg, which is at the high end of an expected rider.

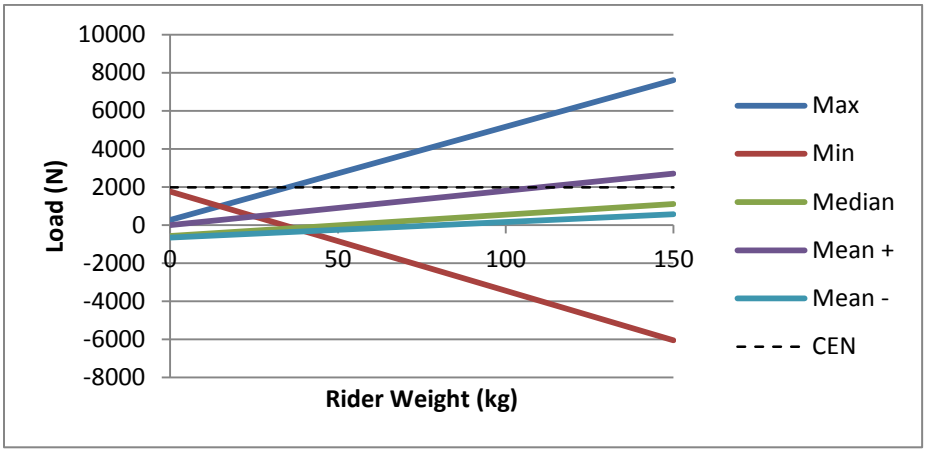

Figure 55: Chain Load Modeled Weight Response and Standardized Test Levels

The BB MX load case seems to err on the side of caution in the standardized tests (Figure 56). The mean loads stay well within the limits of the fatigue test and even the extreme loads do not exceed this limit by much for an average sized rider.

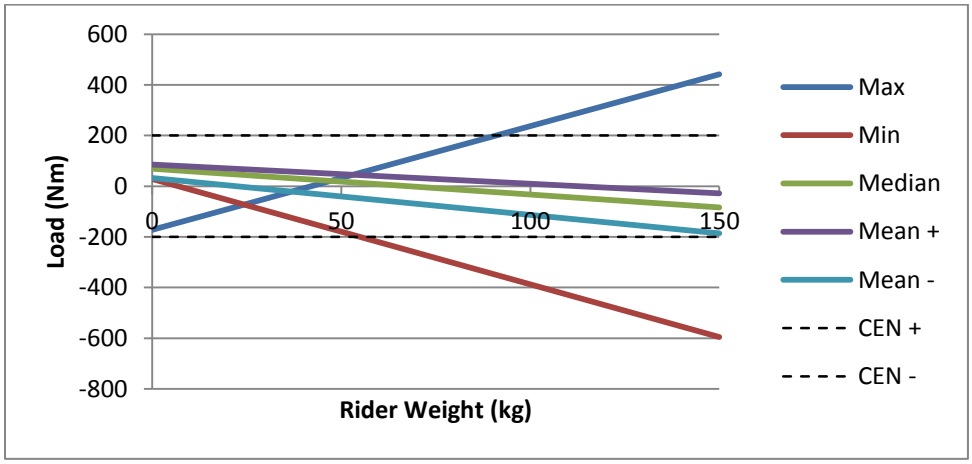

Figure 56: BB MX Modeled Weight Response and Standardized Test Levels

The standard tests for the HT MZ leave a larger margin of safety (Figure 57). Based on the tests conducted, there is no reasonable expectation that a bicycle would ever experience the levels of force required for the fatigue test outside of crash conditions. This confirmed suspicions of some design engineers as, when these standards were adopted, older designs that had never had a head tube failure would consistently fail this test.

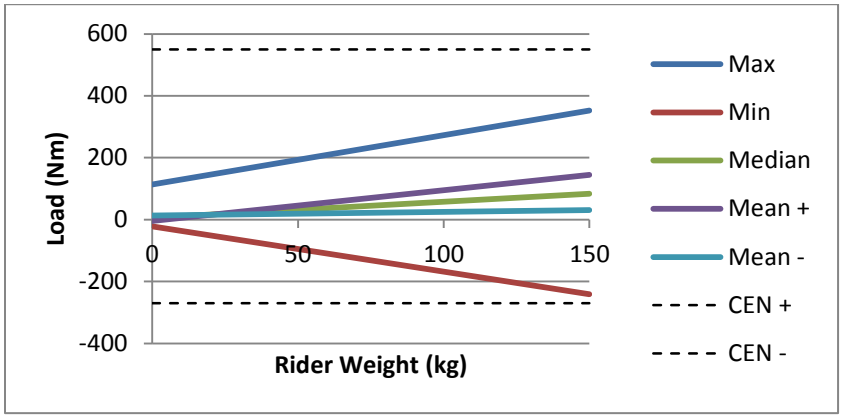

Figure 57: HT MZ Modeled Weight Response and Standardized Test Levels

The final load tested for by the British Standards, is the vertical load on the seat. This, again, seems to be a safely conservative level, but not excessively so. Heavier riders, though, may exceed the limits regularly. This has been corroborated by Rider C as he indicated that he regularly bends or breaks seat-posts.

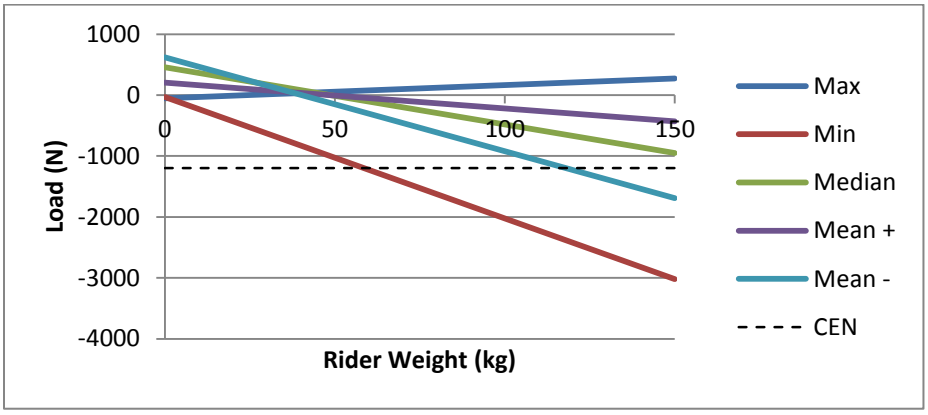

Figure 58: Seat FY Modeled Weight Response and Standardized Test Levels

There are two loads that were tested for that are not represented in the standard fatigue testing at all. The brake load and the HT MX load. Both of these were found to be significant loads that could potentially lead to failures if not considered in design.

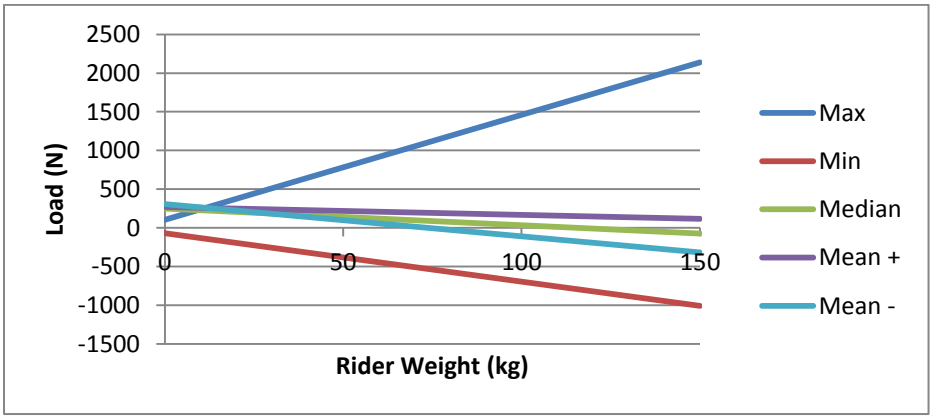

Figure 59: Brake Load Modeled Weight Response and Standardized Test Levels

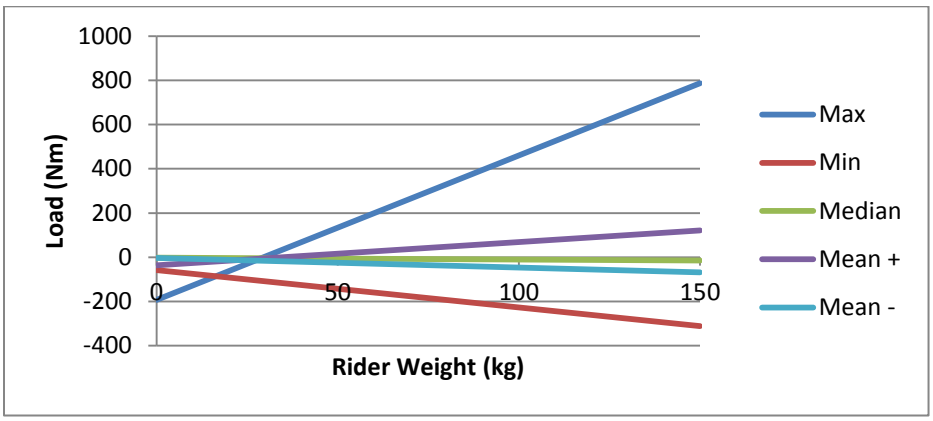

Figure 60: HT MX Modeled Weight Response and Standardized Test Levels

Chapter 7
Conclusions

7.1 Summary

The [j] matrix method of determining load states from strain measurements on a rigid bicycle frame has been shown to be effective. Precision in the development of the [k] matrix has been found to be essential if the system is to be accurate. The system developed was able to resolve most loads to within 20% of the measured load 90% of the time.

There are significant limitations on the system, however. Loads on extremely rigid frames or load cases to which a frame does not meaningfully deflect cannot be effectively measured by the system as it relies on differential strain readings, which are too small to measure in these cases. Also, significant changes in geometry, such as those caused by the compression of rear shocks in a bicycle frame, are not easily accommodated.

Tests of riders of varied sizes on a cross-country course confirm the linear relationship between rider weight and applied moment about the bottom bracket as found by Stone and Hull [19] and expand that relationship to include loading directions on mountain bicycles. An exception to this was found in the load applied at the bottom bracket, orthogonal to the plane of the bicycle. This load showed no relationship with rider height or weight.

Results of the cross country test rides indicate that the standardized tests required for European sales of bicycles are inconsistent with the loads experienced in riding. The moments about the bottom bracket may be somewhat conservative as is the test for the seat load. Conversely, the moment about the head tube caused by fork splay has a factor of safety that may be excessive, and does not appear to represent actual ride conditions.

The moment about the head tube relative to the rear axle and fatigue loading due to braking were also found to be significant cyclic loads in riding, but are not represented in the standardized test procedures.

7.2 Directions for Further Research

The most obvious next step for refining the [k] matrix, strain-gauge method for use on mountain bicycles, is to create a robust means for determining the compression of the rear shock. This would push the results into a range of accuracy that could produce very valuable usage values for design purposes.

To further improve the accuracy, building an even more robust test fixture with at least 1N resolution would improve the precision of the [k] matrix and its results significantly. Improvements beyond this are likely not possible as the precision of the entire system would be passing the precision of the data acquisition system.

Another important direction that this research could be taken, is laboratory life-cycle testing. A fixture could be developed that could apply the load profiles acquired from riding to a frame in real-time. This would facilitate fatigue testing with near-perfect fidelity to actual riding. Benefits to this include comparing frame performance based on different riders, different styles (cross-country, downhill, etc.), and also, different levels of damage. For example, a new frame could be tested in comparison to one that had experienced a serious, but non catastrophic crash, or one with a chip in it. The results of these tests could be very useful for warrantee prediction as well as frame design purposes.

Appendix A

FEA Analysis Images

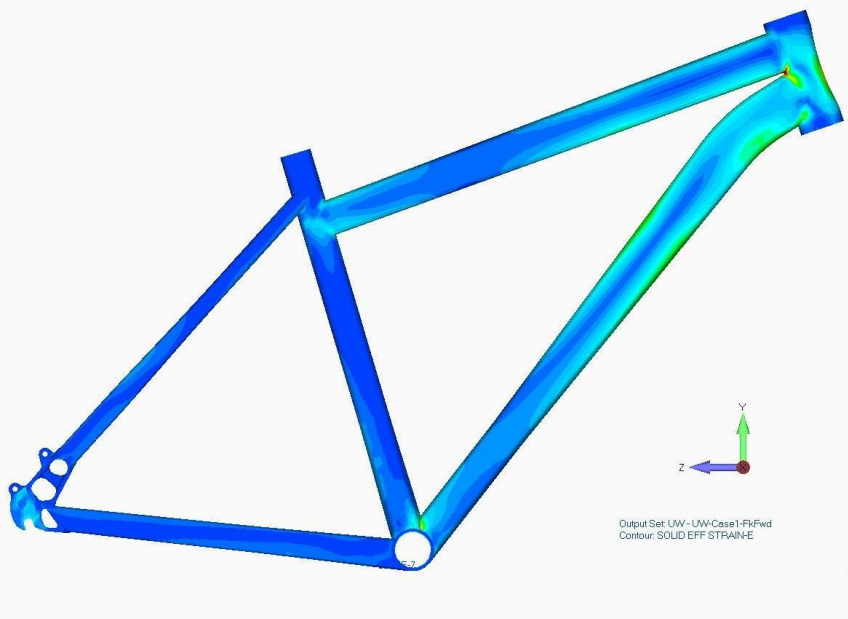

Figure 61: Vertex FEA HT MZ

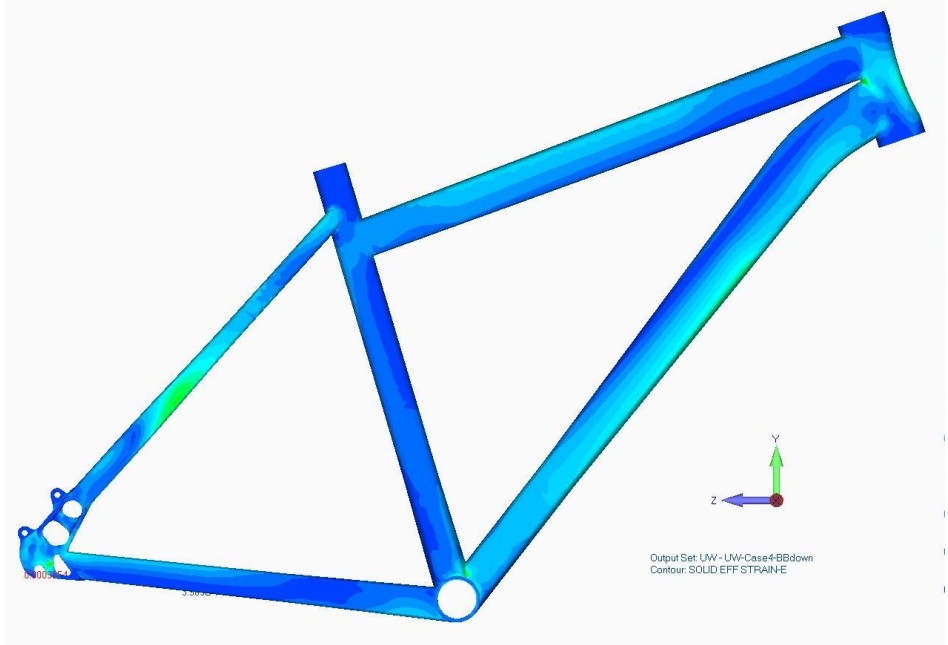

Figure 62: Vertex FEA BB FY

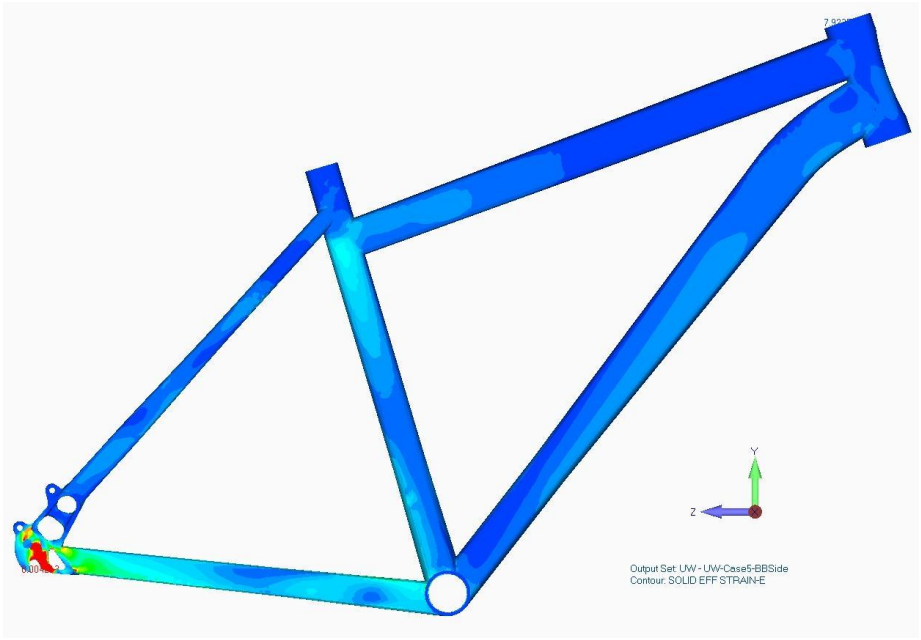

Figure 63: Vertex FEA BB FZ

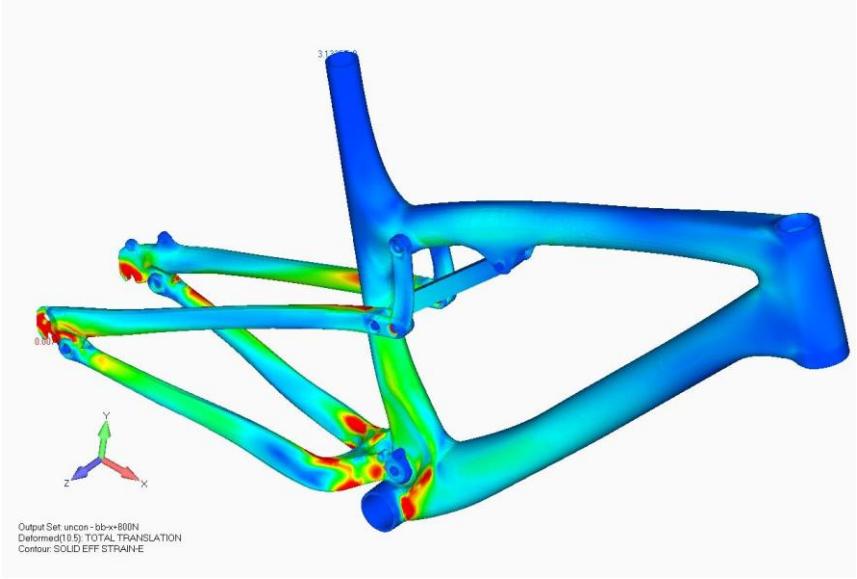

Figure 64: Element FEA BB MX

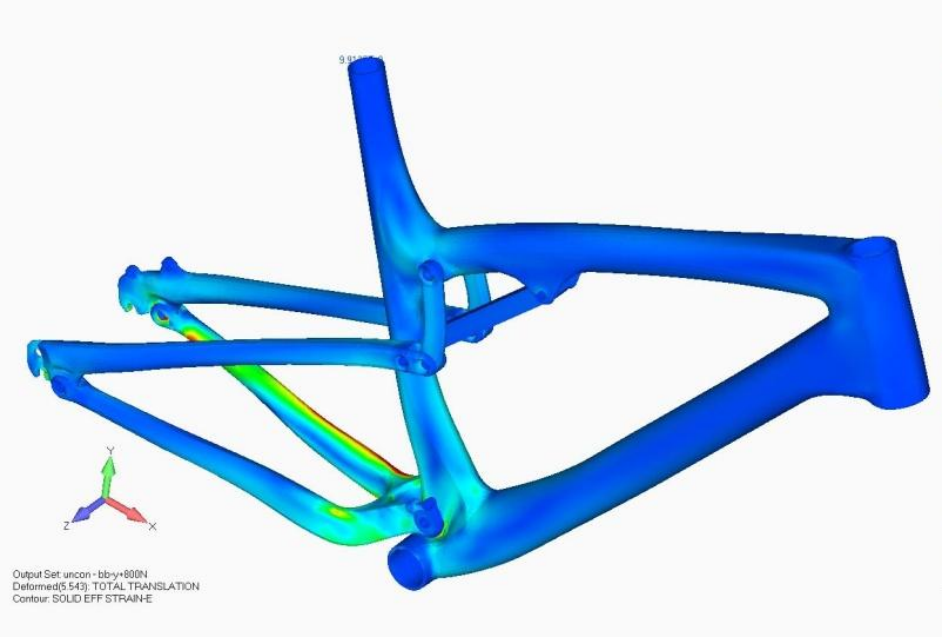

Figure 65: Element FEA BB MY

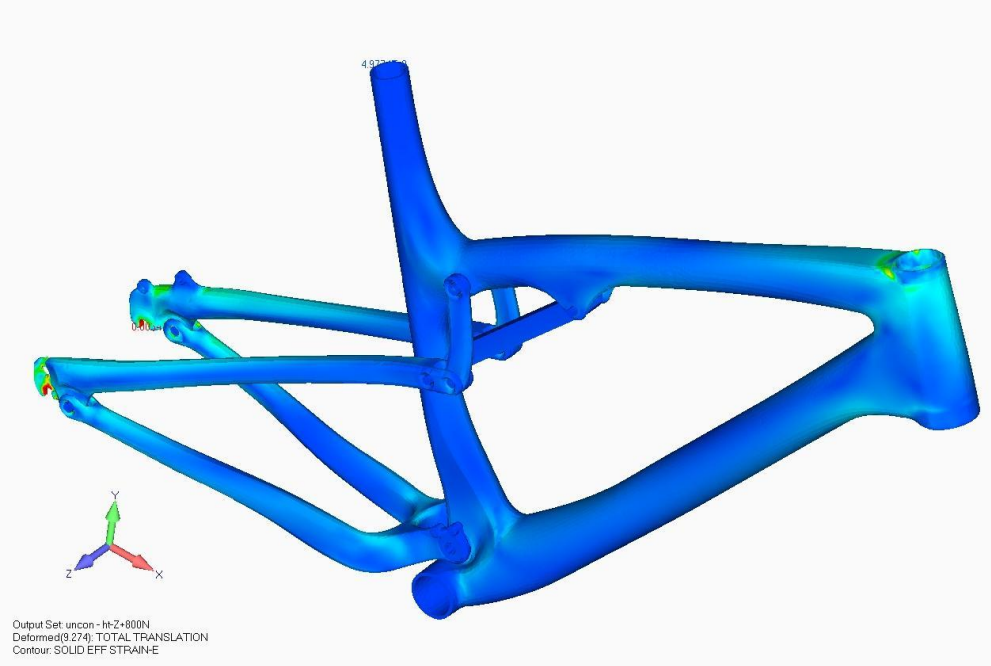

Figure 66: Element FEA HT MZ

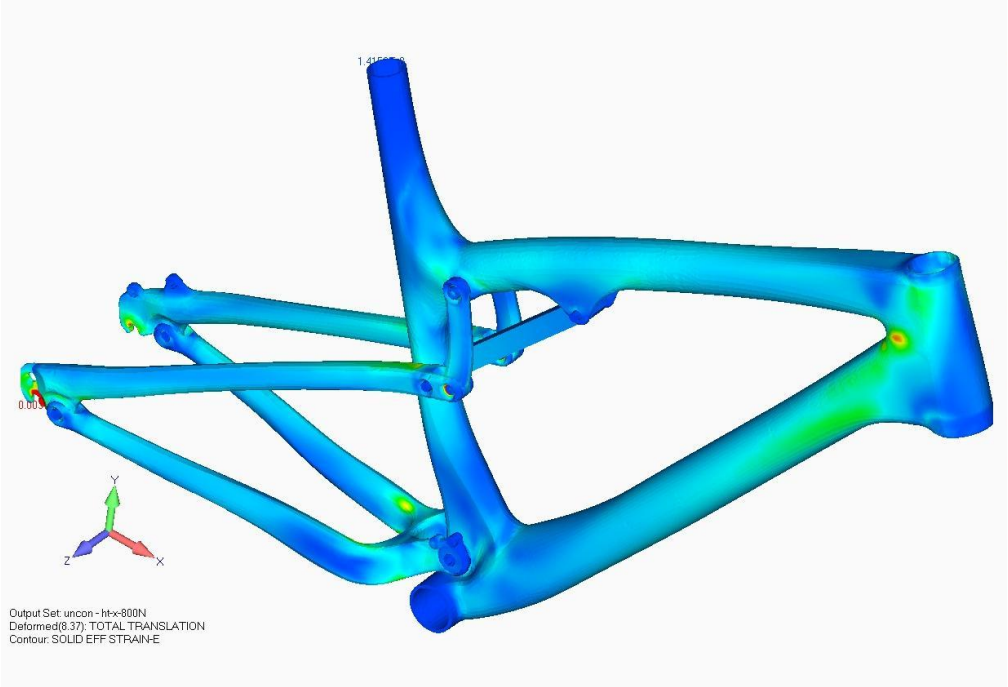

Figure 67: Element FEA HT MX

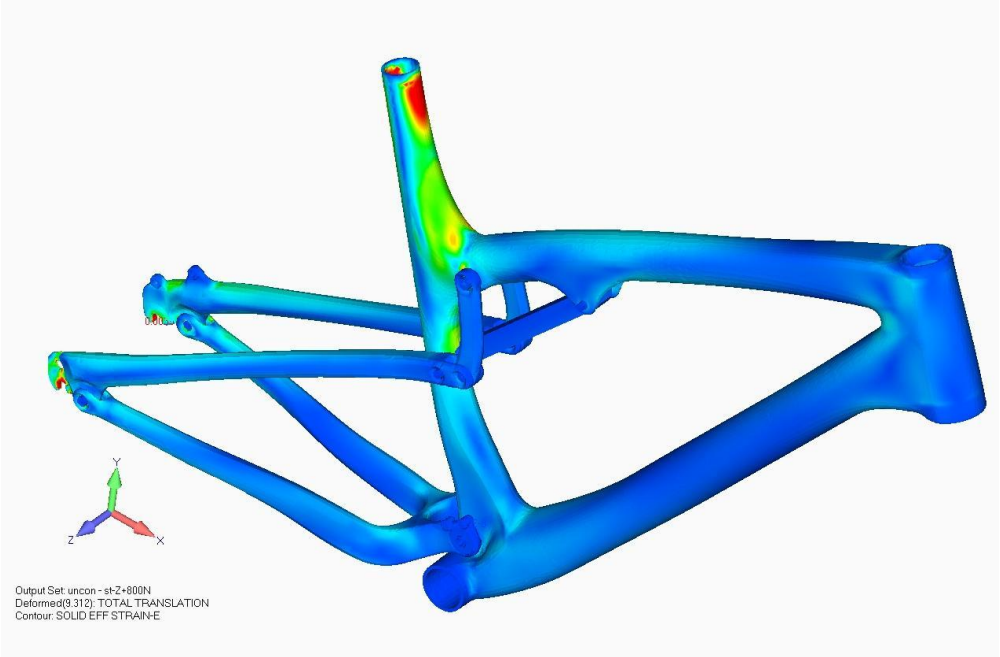

Figure 68: Element FEA Seat FZ

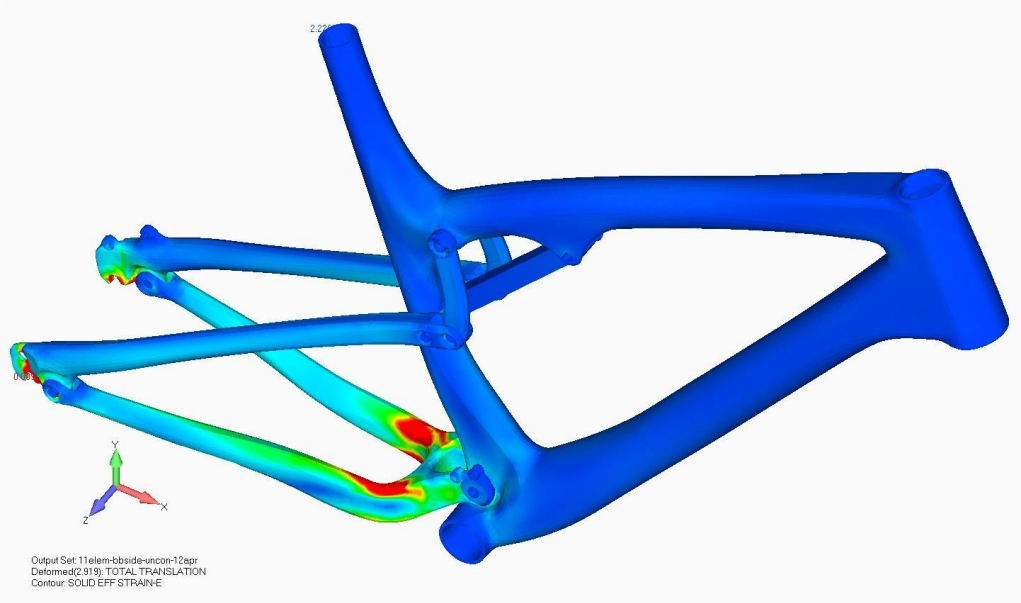

Figure 69: Element FEA BB FZ

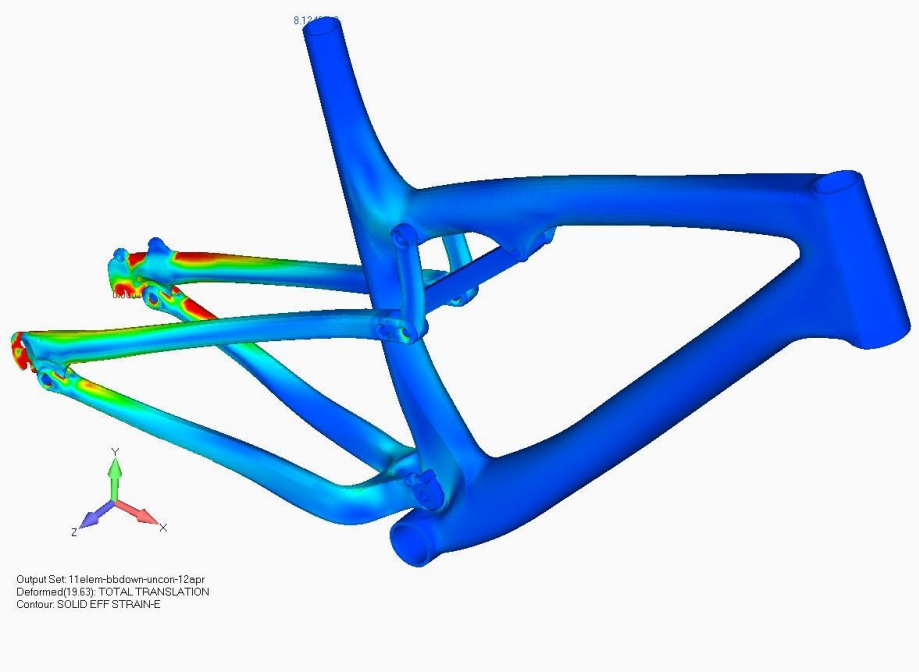

Figure 70: Element FEA BB FY

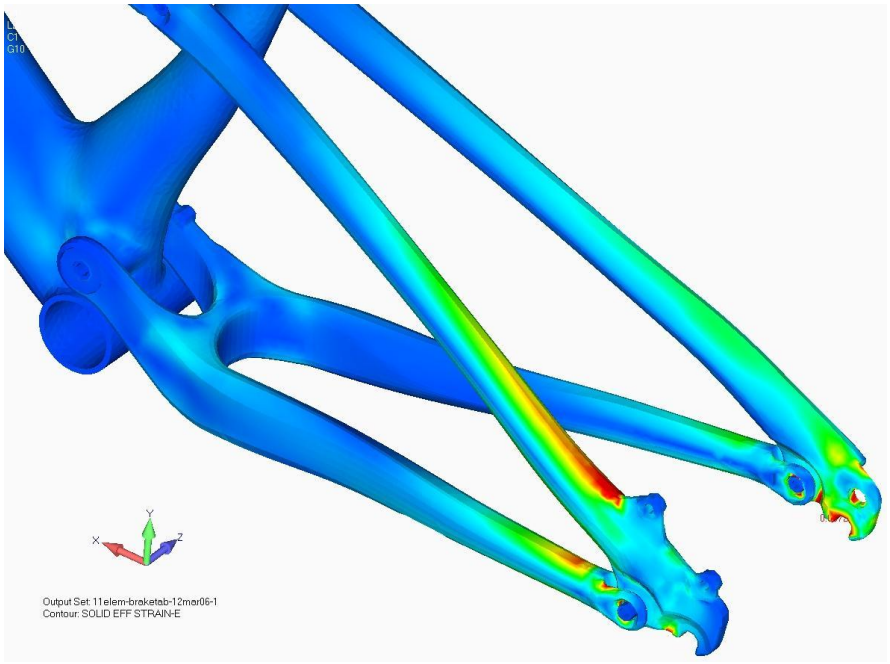

Figure 71: Element FEA Brake Tab

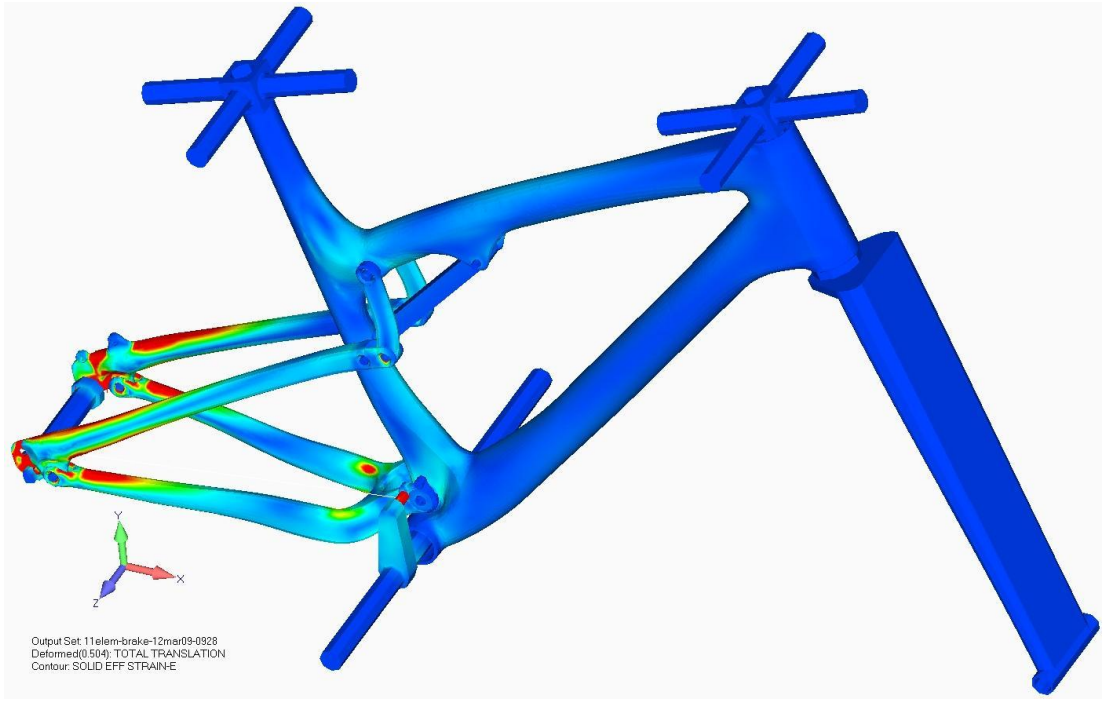

Figure 72: Element FEA Chain Load

Appendix B

Rider Weight Model Data

HTMZ

Weight	Max	Min	Median	Mean +	Mean -
70	250	-100	47	24	-21
70	232	-174	40	24	-21
84	219	-142	45	32	-31
84	223	-108	50	24	-22
105	320	-121	65	41	-33
105	273	-227	61	40	-34
105	267	-193	56	39	-37
Slope	1.59	-1.46	0.52	1.00	0.12
Intercept	114	-22	6	-5	13

SEAT

Weight	Max	Min	Median	Mean +	Mean -
70	163	-1662	-183	123	-306
70	41	-1442	-259	133	-272
84	164	-1445	-380	187	-285
84	88	-1581	-228	119	-304
105	163	-1939	-471	256	-465
105	210	-2291	-612	328	-460
105	154	-2268	-511	297	-511
Slope	2.18	-19.90	-9.37	-4.24	-15.41
Intercept	-54	-34	456	206	621

Brake

Weight	Max	Min	Median	Mean +	Mean -
70	931	-401	79	92	-87
70	1113	-481	90	109	-86
84	1505	-444	125	127	-113
84	1110	-973	57	105	-99
105	1451	-698	-32	124	-164
105	1571	-721	55	154	-157
105	1492	-660	31	142	-138
Slope	13.54	-6.28	-2.17	-1.01	-4.16
Intercept	106	-67	251	270	308

BBMX

Weight	Max	Min	Median	Mean +	Mean -
70	133	-258	2	35	-67
70	99	-271	-7	34	-68
105	421	-557	-42	40	-75
105	146	-335	-52	44	-83
105	199	-327	-17	48	-90
Slope	4.09	-4.16	-1.02	-0.75	-1.46
Intercept	-172	28	69	85	33

HT MX

Weight	Max	Min	Median	Mean +	Mean -
70	286	-147	-8	47	-25
70	251	-160	-4	63	-26
84	449	-316	-15	49	-36
84	261	-162	-10	44	-26
105	697	-236	-7	100	-35
105	383	-240	-16	73	-43
105	392	-197	-8	93	-35
Slope	6.53	-1.69	-0.09	1.04	-0.44
Intercept	-193	-58	-2	-36	-3

CRANK

Weight	Max	Min	Median	Mean +	Mean -
70	3607	-621	176	1104	-294
70	4146	-709	339	984	-302
84	4263	-7602	179	1265	-402
84	3981	-1777	404	1070	-258
105	5045	-7558	644	1286	-360
105	6197	-780	693	1168	-394
105	5131	-1051	511	1400	-445
Slope	48.96	-52.02	11.24	18.12	8.20
Intercept	269	1757	-579	-9	-660

BBMY

Weight	Max	Min	Median	Mean +	Mean -

70	75	-155	-14	17	-30
70	57	-173	-14	19	-33
84	485	-187	-17	23	-42
84	544	-158	-7	20	-36
105	115	-235	1	35	-68
105	153	-213	-6	39	-75
105	115	-181	-10	35	-56
Slope	-1.03	-1.40	0.27	0.84	-0.78
Intercept	312	-62	-34	-57	12

BBFZ

Weight	Max	Min	Median	Mean +	Mean -
70	948	-692	-39	92	-91
70	783	-553	-34	116	-87
84	2840	-1300	-50	128	-113
84	5230	-790	-42	96	-97
105	2914	-755	-36	109	-79
105	469	-779	-59	83	-82
105	876	-920	-47	126	-117
Slope	-3.39	-3.43	-0.29	-0.27	-0.30
Intercept	2311	-522	-18	87	-113

BBFY

Weight	Max	Min	Median	Mean +	Mean -
70	2586	-2425	0	192	-190
70	1812	-2425	-2	181	-180
84	19402	-3873	-8	337	-357
84	9802	-2359	0	197	-181
105	18969	-7477	-11	260	-252
105	1912	-2742	-5	302	-316
105	3228	-3786	-4	374	-392
Slope	104.09	-67.18	-0.16	3.31	-3.92
Intercept	-1016	2392	10	-35	78

References

[1] "The Active Outdoor Recreation Report, Bicycling," Outdoor Industry Foundation, Boulder, 2006.

[2] "Mountain-bicycles: Safety Requirements and Test methods," British Standard BS EN 14766, 2006.

[3] "City and trekking bicycles. Safety requirements and test methods," BS EN 14764:2005, 2006.

[4] "Racing bicycles. Safety requirements and test methods," BS EN 14781:2005, 2006.

[5] Rocky Mountain Bicycles, Rocky Mountain Bicycles 2012 Catalogue, Rocky Mountain Bicycles, 2012.

[6] "Element Team Frameset," Silverfish, 2006. [Online]. Available: http://www.silverfish-uk.com/cms-files/141-0-full-element-team-frame-1.jpg. [Accessed 5 October 2012].

[7] W. Rankine, "On the Dynamical Principles of the Motion of Velocipedes," *Th Engineer*, vol. 28, pp. 79,129,153,175, 1869.

[8] M. L. Hull and R. R. Davis, "Measurement of Pedal Loading in Bicycling: I. Instrumentation," *J. Bilmechanics,* vol. 14, no. 12, pp. 843-856, 1981.

[9] T. Boyd, M. L. Hull and D. Wootte, "An Improved Accuracy Six-Load Component Pedal Dynamometer for Cycling," *j. Biomechanics,* vol. 29, no. 8, pp. 105-1110, 1996.

[10] J. Newmiller, M. L. Hull and F. E. Zajac, "A Mechanically Decoupled Two ForceComponent Bicycle Pedal Dynamometer," *J. Biomechanics,* vol. 21, no. 5, pp. 375-386, 1988.

[11] Y. Champoux, J. Drouet and S. Dorel, "Development of Multi-platform Instrumented Force Pedals for Track Cycling," in *The Engineering of Sport 7*, Paris, Springer, 2008, pp. 263-271.

[12] M. L. Hull and D. S. De Lorenzo, "A Hub Dynamometer for Measurement of Wheel Forces in Off-Road Bicycling," *Transactions of the ASME,* vol. 121, pp. 132-137, 1999.

[13] Y. Champoux and J. Drouet, "A Novel Dynamometric Buset Design to Measure Wheel Loads in Road Cycling," *Precedia Engineering 2*, pp. 2925-2930, 2010.

[14] M. L. Hull, M. R. Hilland and S. P. McKenna, "Methods for Fatigue Testing Off-Road Bicycle Handlebars Based on Assembly Effects Using Two Different Stem Designs," *J. of Testing and Evaluation,* vol. 31, no. 2, pp. 1-10, 2003.

[15] Y. Champoux, P. Vittecoq, P. Maltais, E. Auger and B. Gauthier, "Measuring the Dynamic Structural Load of an Off-Road Bicycle Frame," *Experimental Techniques,* no. May/June, pp. 33-36, 2004.

[16] R. Giannetti, F. Chichi and P. Erzegovesi, "Low-Cost Lightweight Strain Measurement System for Bycycle Application," *IEEE Transactions on Intrumentation and Measurement,* vol. 47, no. 4, pp. 893-899, 1998.

[17] P. D. Soden and B. A. Adeyefa, "Forces Applied to a Bicycle During Normal Cycling," *J. Biomechanics*, vol. 12, pp. 527-541, 1979.

[18] M. L. Hull and D. S. Lorenzo, "Quantification of Structural Loading During Off-Road Cycling," *J. of Biomechanical Engineering,* vol. 121, pp. 399-405, 1999.

[19] C. Stone and M. L. Hull, "The Effect of Rider Weight on Rider-Induced Loads During Common Cycling Situations," *J. Biomechanics*, vol. 28, no. 4, pp. 365-375, 1995.

[20] M. L. Hull and F. Bolourchi, "Contributions of Rider Induced Loads to Bicycle Frame Stresses," *J. Strain Anal. ,* vol. 23, pp. 687-703, 1988.

[21] C. Hölzel, F. Hoechtl and V. Senner, "Operational Loads on Sport Bicycles for Possible Misuse," *Procedia Eng.*, vol. 13, pp. 75-80, 2011.

[22] S. I. Grossman, in *Elementary Linear Algebra, 5th Edition*, Philadelphia, Saunders College Publishing, 1994, p. 421.

[23] Rocky Mountain Bicycles, "bikes.com," 2009. [Online]. Available: http://www.bikes.com/DATA/BIKE/527_en.pdf. [Accessed 5 October 2012].

[24] National Instruments Corporation, "Developer Zone: Strain Gauge Configuration Types," National Instruments Corporation, 2012. [Online]. Available: http://www.ni.com/white-paper/4172/en. [Accessed 15 October 2012].

[25] A. Nieslony, "MatLab Central - Rainflow Counting Algorithm," 04 April 2010. [Online]. Available: http://www.mathworks.com/matlabcentral/fileexchange/3026-rainflow-counting-algorithm. [Accessed 6 March 2012].

[26] Lead Dog Visual Arts, "Hydrocut Map," 23 October 2012. [Online]. Available: http://waterloocyclingclub.ca/wp-content/uploads/2012/01/HydrocutMap.pdf. [Accessed 25 October 2012].